Marine and Petroleum Geology 140 (2022) 105644

Contents lists available at ScienceDirect

Marine and Petroleum Geology

journal homepage: www.elsevier.com/locate/marpetgeo

Secondary porosity development in incised valley sandstones from two wells from the Flemish Pass area, offshore Newfoundland

John B. Gordon [a,*], Hamed Sanei [b], Per K. Pedersen [a]

[a] Department of Geoscience, University of Calgary, 2500 University Drive NW, Calgary, AB, T2N 1N4, Canada
[b] Lithospheric Organic Carbon (LOC) Group, Department of Geoscience, Aarhus University, Høegh-Guldbergs Gade 2, Building 1671, 223, 8000, Aarhus C, Denmark

ARTICLE INFO

Keywords:
Organic petrology
Secondary porosity
Diagenesis
Petrography

ABSTRACT

In this study we discuss the diagenetic processes that have contributed to the preservation of anomalously high secondary porosity (20–30%) and associated high permeability in relative deeply buried (2–3 km) Tithonian-aged stacked incised valley reservoir sandstone intervals (informally named Ti-2 and Ti-3) in the Flemish Pass area, offshore Newfoundland. These incised valley sandstones are bounded by thick organic-rich and/or organic-lean siltstone and mudstone deltaic deposits. Here we use a multi disciplinary approach including thin section petrography, cathodoluminescence (CL) petrography, programmed pyrolysis, and organic petrology to examine the controls on organic matter and secondary porosity development in the studied sandstones. The incised valley sandstones are dominated by litharenites, sublitharenites, and feldspathic litharenites. The most significant early diagenetic pore-occluding event is pervasive poikilotopic calcite cementation that arrested the affects of mechanical compaction preserving framework grains in point contact. Secondary porosity formed by dissolution of the calcite cement is commonly speculated to be related to thermal maturation of organic matter (OM) and associated generation of short-chained carboxylic acid (SCCA). %VRo data shows the OM to be immature (0.5%) therefore the estimated burial temperature of the sediment likely never got above approximately 60 °C in the late diagenesis to early catagenesis stage. This thermal maturity is consistent with the pre-oil generation window and the onset of SCCA generation allowing early calcite dissolution to take place. It is likely a second phase of meteoric water flushing took place, however, the scale of investigation of this study was not adequate to verify meteoric water flushing as a mechanism for calcite cement dissolution.

1. Introduction

Secondary porosity refers to the pore space in a reservoir rock that resulted from post-depositional processes that caused detrital grains and/or diagenetic cements to dissolve, as first recognized and described based on qualitative observations from thin sections (Schmidt and Mcdonald, 1979). The existence of secondary porosity in hydrocarbon reservoirs has been a key interest to oil and gas companies for decades as anomalous high porosity values have been reported globally in deeply buried (>2 km) sandstones reservoirs. Significant increase in porosity by the dissolution of minerals, especially in the case of grain dissolution of feldspars and pore-filling carbonate cements, has been documented in diagenetic literature for more than forty years (Schmidt and Mcdonald, 1979; Surdam et al., 1984; Surdam and Crossey, 1985; Burley and Kantorowicz, 1986; Gluyas and Coleman, 1992; Hansley and Nuccio, 1992; Burley and Worden, 2003; Xiong et al., 2016; Olanipekun and Azmy, 2021). However, questions exist concerning the mechanisms that contribute to secondary porosity generation, especially by carbonate cement dissolution. This disagreement is based on the physical and chemical interactions that have to occur in terms of the mass transfer of large amounts of solids and geochemical variability at these deep burial depths in a closed system (Lundegard et al., 1984; Bjørlykke and Jahren, 2012; Bjørlykke 2014; Taylor et al., 2010; Yuan et al., 2019).

The Tithonian-aged (Ti) reservoir sandstones of the Flemish Pass, offshore Newfoundland are the current target of hydrocarbon exploration due to the abundant well preserved anomalously high secondary porosity in these deeply buried (~3 km) sandstone units. Five stacked potential reservoir units have been identified to date in the Flemish Pass bounded by thick silt and/or mudstone intervals (base to top Ti-0 to Ti-4; Haynes et al., 2014). The Ti-3 and Ti-2 sandstones have been interpreted as the fill of incised valleys that formed in response to base level falls related to syn-rift extension that led to the creation of incised valley

* Corresponding author.
E-mail address: john.gordon1@ucalgary.ca (J.B. Gordon).

https://doi.org/10.1016/j.marpetgeo.2022.105644
Received 8 November 2021; Received in revised form 6 March 2022; Accepted 10 March 2022
Available online 15 March 2022

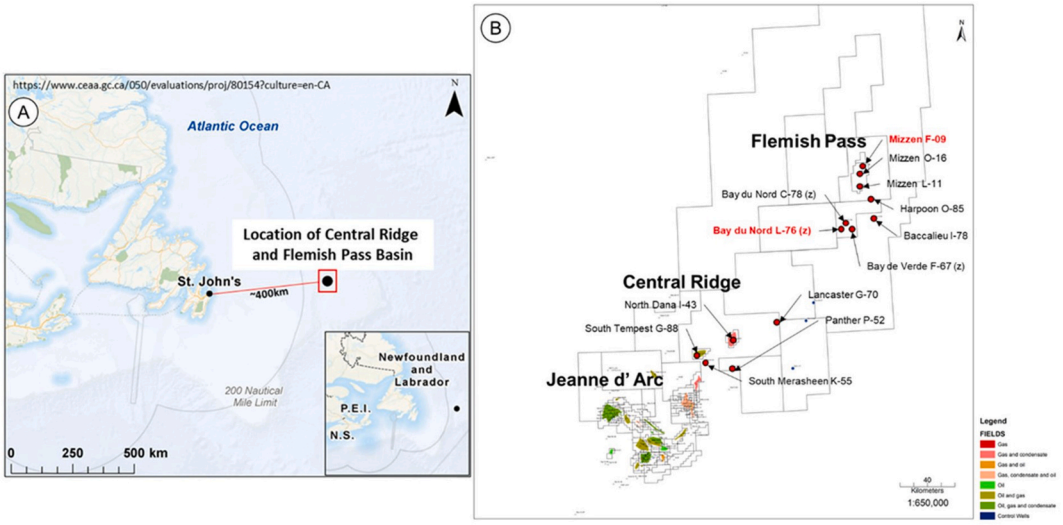

Fig. 1. A) Map showing location of the Flemish Pass Basin approximately 400 km east of St. John's Newfoundland, Canada. B) Closer view map of the Jeanne d' Arc Basin, Central Ridge, and Flemish Pass Basin. Flemish Pass wells in this study are highlighted in red font (map supplied by Husky Energy Inc.). (For interpretation of the references to colour in this figure legend, the reader is referred to the Web version of this article.)

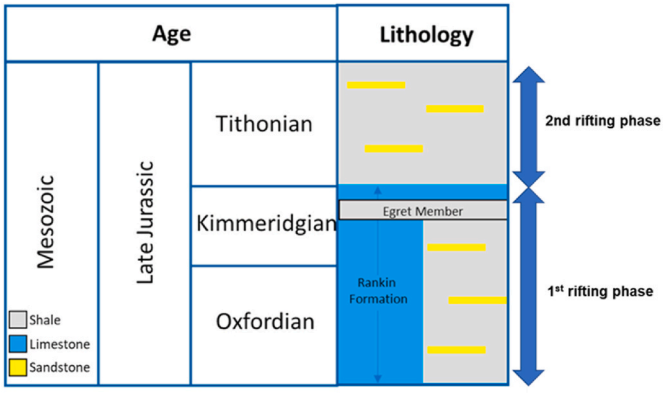

Fig. 2. Jeanne d' Arc lithostratigraphic chart showing the Tithonian intervals of interest. The Kimmeridgian-aged Rankin Formation and the Egret member are highlighted (Modified from Enachescu, 2005; Gordon et al., 2021). First stage of rifting began in the early Upper Jurassic and continued to the late Tithonian causing the formation of horst and grabens where clastic sediment fills the grabens. Second stage of rifting continues to fill grabens with clastic sediment shedding from above sea level horst structure (Beicip Franlab, 2018). Rifting continues into the Cretaceous.

systems (Stewart, 2016; unpublished). These valleys were backfilled with fluvio-marine sediments during transgression and have been identified as potential oil reservoir targets due to their high secondary porosity and high permeability. Previous studies in this area have focused on the structural and depositional history of these sandstones (Haynes et al., 2014; Beicip Franlab, 2015, 2018), however the evolution and preservation of secondary porosity is rarely reported in the literature. The main contributor to secondary porosity in the Flemish Pass sandstones has been suggested to be short-chained carboxylic acids (SCCA) generated during thermal maturation of organic matter (OM; Hesse and Abid, 1998; Xiong et al., 2016), but limited geochemical evidence has been reported to support this interpretation.

In this study, we examined samples from two wells in the Flemish Pass area. We used a multidisciplinary approach using thin section petrography, cathodoluminescence (CL) petrography, programmed pyrolysis, and organic petrology. The objectives of this study are to: (i) examine the pore-filling calcite cement in the Ti2 and Ti-3 incised valley sandstones to better understand the origin and occurrence of the calcite cement, (ii) construct a paragenetic sequence of diagenetic events, (iii) investigate the type, distribution, and thermal maturity of the OM found in the organic-rich silt and/or mudstone units enveloping the Ti-3 and Ti-2 incised valley sandstones as well as the interbedded organic-rich layers within the Ti-3 and Ti-2 incised valley sandstones, and (iv) attempt to shed light on the possible mechanisms that control secondary porosity development in these Tithonian-aged incised valley sandstones.

2. Geological background

The two wells in this study (Mizzen F-09 and Bay du Nord L-76z) were drilled in the Flemish Pass area located off the east coast of Newfoundland approximately 480 km east of St. John's (Fig. 1). The Flemish Pass sub-basin formed in response to Late Triassic to Paleocene rifting events that formed deep sedimentary basins bounded by faults (Creaney and Allison, 1987; Enachescu, 2005). An initial rifting phase in the Late Triassic to Early Jurassic and a second phase rifting event from Later Jurassic to Early Cretaceous led to deposition of widespread sandstone reservoirs within the half graben fault blocks (Enachescu, 1987; Foster and Robson, 1993; Sinclair et al., 1994). Fig. 2 shows a simplified lithostratigraphic chart showing Tithonian sands and rifting phases of interest to this study.

In 2003 Mizzen L-11 was drilled by Petro Canada Oil and Gas and confirmed the presence of good quality reservoirs in Tithonian-aged sandstones but was deemed uneconomic. Mizzen O-16 was drilled in 2008 by Statoil Canada and was announced as an oil discovery that spawned new interest in the Mizzen, Harpoon, Bay du Nord, and Bay du Verde areas (Beicip Franlab, 2018). Mizzen F-09 was drilled in 2011 and Bay du Nord L-76z in 2015 by Statoil Canada and Husky Oil Operations. Bay du Nord L-76z was listed as a significant discovery by the Canada-Newfoundland and Labrador Offshore Petroleum Board (C-NLOPB) in 2017. Both wells encountered good to excellent reservoir units in Tithonian-aged sandstones. However, a substantial amount of calcite cement is present in the Ti-3 sandstone unit in Mizzen F-09 severely reducing reservoir quality.

Five defined meter to dekameter-scale and unconformity-bounded sandstone intervals (informal names from base to top Ti-0 to Ti-4; Haynes et al., 2014) are sharply underlain and overlain by deltaic organic-rich and/or organic-lean siltstones and mudstones. The depositional environment has been described as fluvial to deltaic facies (delta front to pro-delta deposits; Beicip Franlab, 2015), whereas Haynes et al.

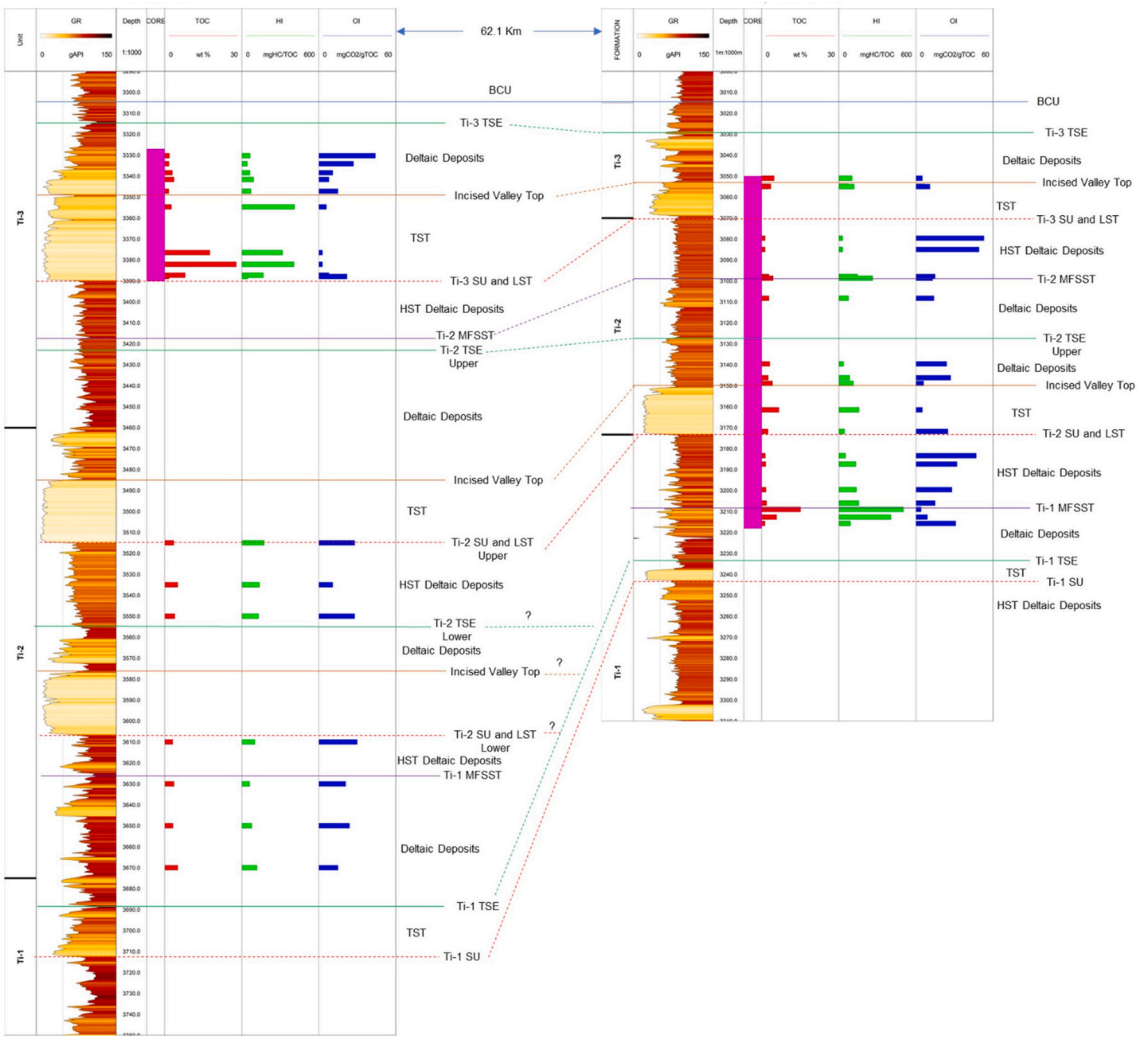

Fig. 3. A simplified cross section of the two wells from this study. The Tithonian secessions can be divided into five unconformity-bounded sequences in the Flemish Pass area (Ti-0 to Ti-04). The Ti-3 and Ti-2 incised valley sandstones are the main interest to this study. See text for details. (modified Stewart, 2016 unpublished).

(2014) interpreted the sandstones as synrift braided fluvial channel belts.

These stacked cyclic patterns of the Ti siltstones/mudstones and sandstones were placed in a sequence stratigraphic context by Stewart (2016; unpublished). Each Ti depositional sequence begins with a basal subaerial unconformity (SU), that marks the base of an incised valley that is cut into the deltaic deposits of the preceding cycle as a result of falling sea level due to tectonic uplift. As sea level begins to rise (due to rift structural relaxation) the transgressing sea backfills the accommodation space in the valley with quartzose and feldspathic sandstones containing abundant shells, oolitic, and carbonate rock fragments. With progressive transgression, the valleys and intervalley areas eventually fill with deltaic sediments. This succession was capped by the transgressive surface of erosion (TSE), above which sediments were deposited in progressively deeper water and clastic-starved conditions until the maximum flooding surface (MFS) is reached. Above the MFS regression started once again, marked by regional prograding prodelta and delta front sediments. These sediments are truncated by the next SU generated by another uplift episode of rift-related tectonics. This cycle is repeated for each of the Ti sequences until the Base Cretaceous Unconformity (BCU) after the Ti-3 sequence. A cross section of the two wells can be viewed in Fig. 3.

In the neighbouring Jeanne d' Arc Basin the Kimmeridgian-aged Egret Member of the Rankin Formation has long been considered the primary source rock (Swift and Williams, 1980; Creaney and Allison, 1987; Fowler et al., 1990, 1991; Huang, 1994; Fowler and McAlpine, 1995; DeSilva, 1999; Enachescu et al., 2010, Enachescu, 2012). The equivalent source rock is preserved in Tithonian-aged sediments throughout other subbasins in offshore Newfoundland including the Flemish Pass (Enachescu, 2005; Fowler et al., 2007; Gordon et al., 2021). This source rock has been described to have an abundance of well preserved autochthonous Type II marine algal OM (Raine, 2006, unpublished) with high total organic carbon (TOC), high hydrogen index (HI), and low oxygen index (OI). Type II marine OM is deposited during the sea level rise within the incised valley sandstones in thin mm to cm layers. However, this OM type is best preserved in cm to dm thick layers associated with the MFS in the Tithonian sediments. High TOC mixed Type II/III OM are also present but have low HI and high OI due to the abundance of allochthonous derived continental degraded and reworked OM suggestive of a more terrigenous land derived sediment likely derived from a deltaic source (Raine, 2006, unpublished; Gordon et al., 2021).

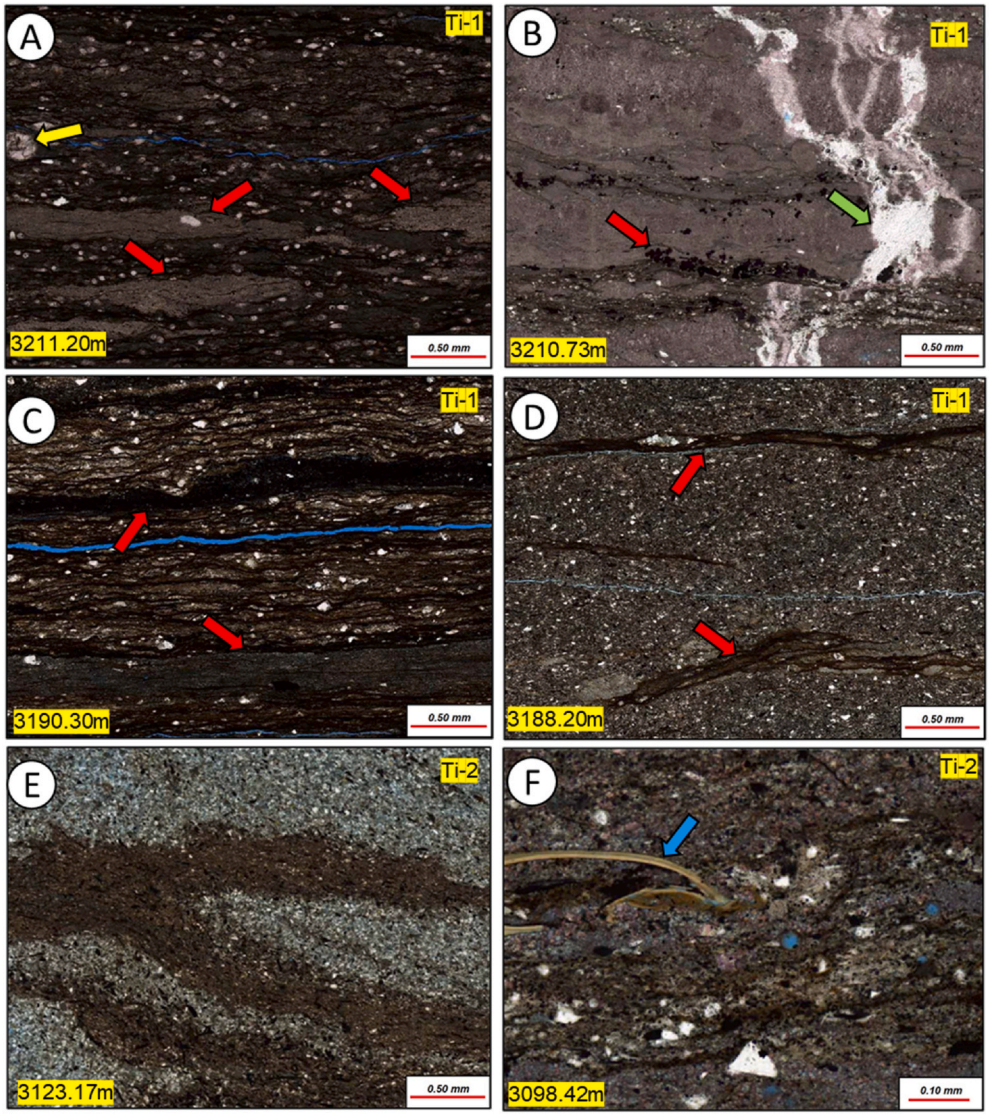

Fig. 4. Representative thin section photomicrographs of Ti-1 (A–D) and Ti-2 (E–F) siltstones and mudstones from Bay du Nord L-76z. Samples are arranged from deepest (A) to shallowest (F). A) Organic-rich lime mudrock. Note compacted mud lenses (red arrows). Small white specs are calcite microfossils (sponge spicules?) and one calcispheres is present (yellow arrow). B) Lime mudrock. Note calcite-healed fracture (green arrow). Discrete organic laminae are present with abundant pyrite (red arrow). C) Similar sample to A but has abundant silt-sized quartz grains with thick condensed organic-rich layers (red arrows). D) Silty mudstone with few muddy organic-rich laminae (red arrows). Matrix is silty and muddy. E) Muddy siltstone showing a convoluted mixture of mud and silty layers. F) Silty mudstone. Some organic layers are still preserved. Abundant silt and sand sized quartz grains are present. Note well preserved phosphatized fossil fragment (blue arrow). (For interpretation of the references to colour in this figure legend, the reader is referred to the Web version of this article.)

3. Methodology

3.1. Thin section petrography, cathodoluminescence (CL) petrography, and core analysis

Twenty-five thin sections prepared from core and sidewall cores (SWC) were borrowed from the C-NLOPB from Mizzen F-09 and six thin sections from Bay du Nord L-76z. Thin section point count data was supplied by Husky Energy Inc. in petrographic reports completed on Mizzen F-09 (File No. NF-52473) and Bay du Nord L-76z (File No. NF-76997) by Weatherford Laboratories in Calgary, Alberta, Canada. Several thin section photomicrographs from these reports were included in this study where no physical thin sections were available in the zones of interest. Core analysis data was supplied by Husky Energy Inc. on one hundred and ninety-six core samples taken from the Bay du Nord L-76z core and one hundred and fifty core samples and eighteen SWC samples from the Mizzen F-09 well. Core analysis was performed on 2.54 cm (diameter) small plugs extracted from the core. Permeability was run at 800 psi confining pressure and porosity measurements were taken at ambient conditions. The thin sections borrowed from the C-NLOPB were of different vintages and were prepared by different unknown laboratories. Therefore, not all samples were prepared the same way and many samples were not stained for carbonate identification. Some of the samples were impregnated with a blue-dyed epoxy and ground to a standard 30-μm thickness. Some samples were stained for potassium feldspar identification (yellow in thin section) and some samples were stained with Alizarin Red-S to identify calcite (pink in thin section), along with potassium ferricyanide to identify ferroan carbonate minerals (blue to purple in thin section). Samples were observed and photographed using a Zeiss Axioscope 10 petrographic microscope. Cathodoluminescence microscopy (CL) was performed on two samples from Bay du Nord L-76z and seven samples from Mizzen F-09 from heavily calcite cemented zones within the reservoir sandstones using a CITL MK5-1 cold cathodoluminescence stage with a 12–15 kV beam and a current intensity of 420–430 μA on the non-stained halves of uncovered thin sections.

3.2. Programmed pyrolysis

Twenty-one samples from Bay du Nord L-76z and eighteen samples from Mizzen F-09 were analyzed for hydrocarbon potential using programmed pyrolysis. The samples were sent to the Lithospheric Organic Carbon (L.O.C.) laboratory, Department of Geoscience, Aarhus University in Denmark, for HAWK pyrolysis analysis using the standard cycle of Rock Eval 6® analysis. The pyrolysis method used was described by Lafargue et al. (1998). Extended Slow Heating (ESH) Slice&Dice®

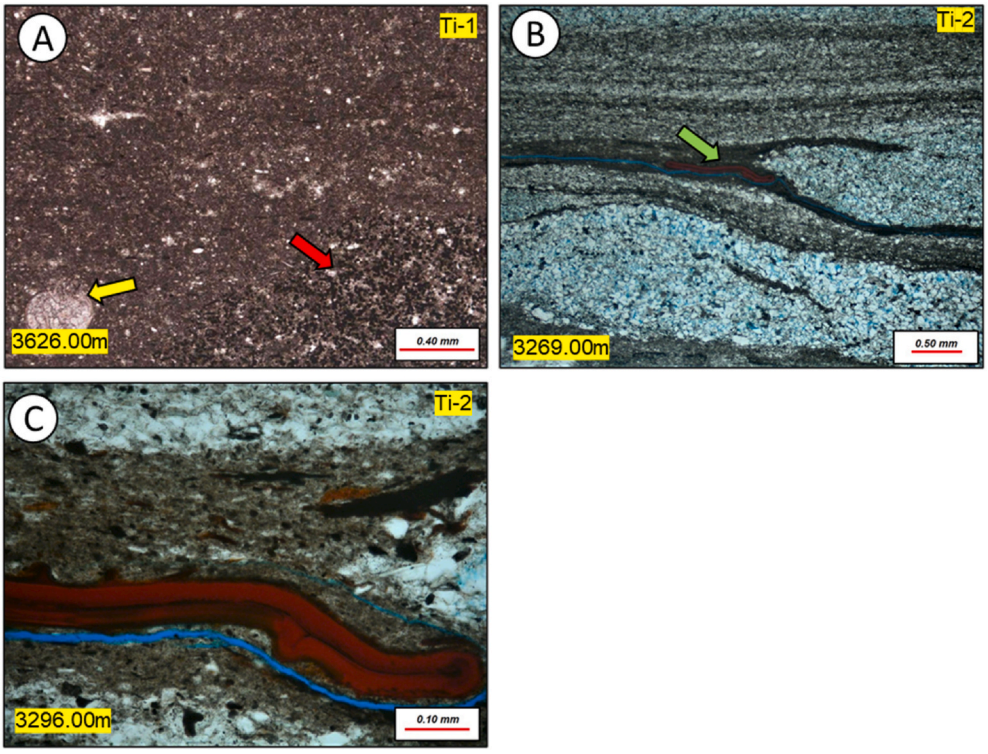

Fig. 5. Representative thin section photomicrographs of Ti-1 (A) and Ti-2 (B and C) siltstones and mudstones from Mizzen F-09. Samples are arranged from deepest (A) to shallowest (C). A) Lime mudstone. Massive with patchy pyrite (red arrow). Note fossil fragment (yellow arrow). B) Bioturbated silty mudstone. Silt-sized clasts are confined to burrow fill. Some organic matter is still preserved. Note well preserved alginite (green arrow). C) Closer view of well-preserved alginite. (For interpretation of the references to colour in this figure legend, the reader is referred to the Web version of this article.)

pyrolysis methods were applied to the programmed pyrolysis data. ESH-Slice&Dice® is a pyrolysis method coupled with an advanced reporting algorithm based on the HAWK Pyrolysis system (Wildcat Technologies, TX, USA). The method was devised by Dr. Hamed Sanei at the Lithospheric Organic Carbon (L.O.C.) Research Centre at the Department of Geoscience at Aarhus University in Aarhus, Denmark. The ESH-Slice&Dice® method provides the most reliable measurements of total free oil/hydrocarbon and hydrocarbon potential of kerogen. The continuous slow heating ramp of 10 °C per minute at a starting temperature of 100 °C provides a clear separation between the entire total oil in the rocks (real S1) from the hydrocarbon potential in non-extractable kerogen (real S2). The extended temperature range and slower heating rate allows sufficient time for the evolution of the hydrocarbon peaks to take place. The separation between the free oil (real S1) peak and thermally cracking hydrocarbon (real S2 kerogen) peak is evolved naturally based on the pyrolysis behavior of the organic compounds in the rock samples which, in turn, are controlled by their molecular composition. This provides a stark advantage over the conventional programmed pyrolysis method, which forces the separation between S1 and S2 at the set iso-temperature of 300 °C, which often does not allow the entire amount of oil to be released and is carried over to the S2. ESH-Slice&Dice® uses a proprietary calibration technique that provides a precise measurement of the real S1 and real S2, without distorting other conventional programmed pyrolysis parameters such as Total Organic Carbon (TOC), Residual Carbon (RC), Oxygen Index (OI), and Pyrolysable Carbon (PC). The calibration provides a great degree of reproducibility and consistency with conventional programmed pyrolysis parameters as carefully monitored by the Wildcat Technologies and IFP standard reference materials (IFP1600 and WT). All pyrolysis data in this study will be reported as ESH-Slice&Dice® values where applicable.

3.3. Organic petrology

Five core samples from Bay du Nord L-76z and three core samples from Mizzen F-09 were selected for organic petrology to verify results from the programmed pyrolysis analysis and to identify organic matter types. The samples were prepared into epoxy-resin sample pellets. The pellets were finely polished, and the analysis was completed on a Zeiss Axioimager II microscope equipped with the Diskus-Fossil system (Hilgers Technisches Buero) for reflectance measurements at the Geological Survey of Canada in Calgary, Canada using an ultrafine measurement probe (0.3 μm^2 spot size) under oil immersion (refractive index, n = 1.518 at 23 °C). An yttrium-aluminum-garnet reference standard was used with a reflectance of 0.906% under oil immersion. The entire surface of the pellet was examined at 50 × magnification to obtain no less than 50 measurements per sample.

Point counting organic macerals was completed using a twenty-one cross-hair grid combined with a motorized automated microscope stage (e.g., Gordon et al., 2021). Organic macerals were counted when intercepted by any of the twenty-one crosses in the field of view. Two hundred maceral counts per sample were counted for maceral distribution under a 50 × oil immersion objective with a maximum of 100× 100 frames per sample. Five groups of macerals (vitrinite, reworked vitrinite, inertinite, liptinite, and bituminite) were determined as described in ICCP (1998), ICCP (2001), Pickel et al. (2017), and Sanei (2020).

4. Results

4.1. Ti-1 – Ti-2 siltstone and mudstone thin section petrography, pyrolysis, and organic petrology

The Bay du Nord L-76z was cored through the entire Ti-2 sequence and portions of the Ti-1 and Ti-3 sequences. In Mizzen F-09 only the Ti-3 incised valley sandstone was cored. Therefore, the petrographic observations of the Ti-1 and Ti-2 siltstone and mudstone units in Mizzen F-09 were from SWC only.

4.1.1. Thin section petrography from the Ti-1 – Ti-2 siltstones and mudstones

In the Bay du Nord L-76z core the Ti-1 and Ti-2 siltstone and mudstone intervals consist of thick grey mudstones with episodic

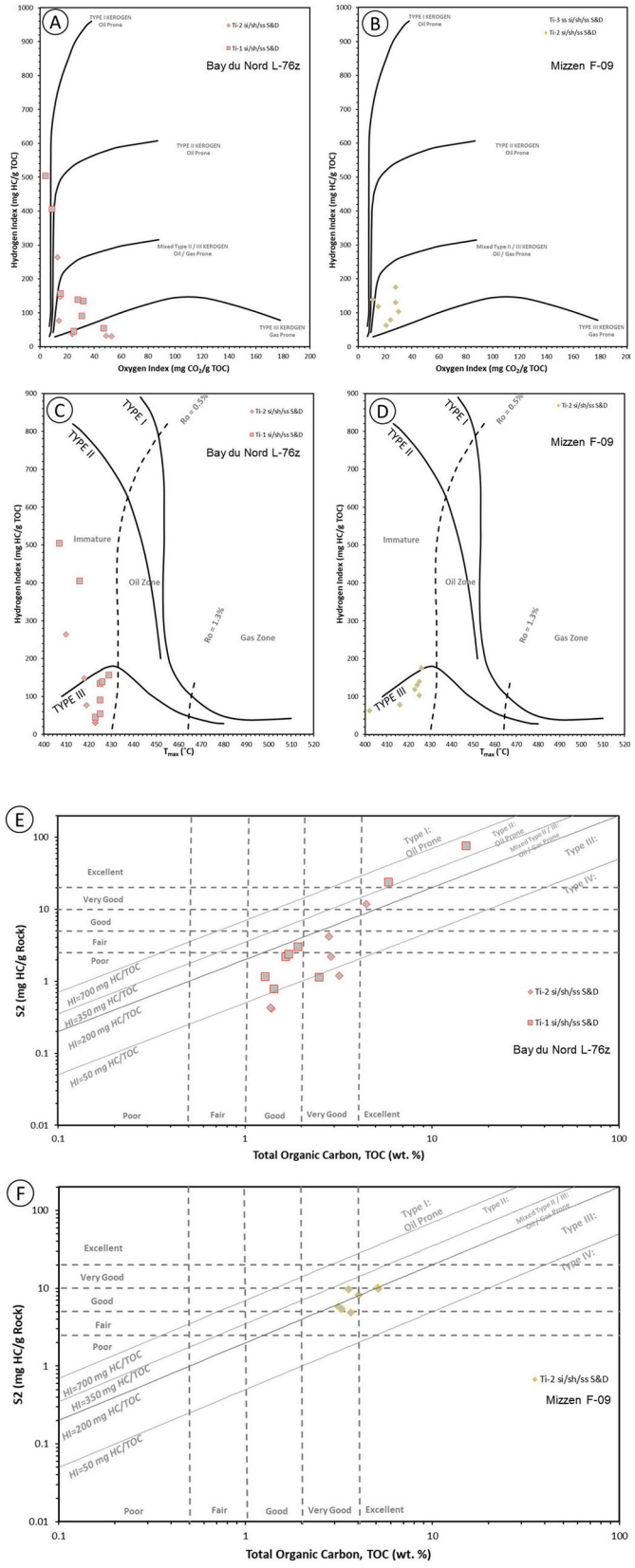

Fig. 6. Pyrolysis data plots for Bay du Nord L-76z Ti-1 and Ti-2 and Mizzen F-09 Ti-2 siltstones and mudstones.

laminae of siltstone and sandstone reflecting oscillations in terrigenous sourced sediments into a marine distal prodelta setting. However, cyclic laminated cm-dm-sized beds of organic-rich lime mudrocks are noted to occur at the MFS's (refer to Fig. 3). Representative thin section photomicrographs of the Ti-1 and Ti-2 siltstones and mudstones from the Bay du Nord L-76z core are shown in Fig. 4 and described below.

The sample at 3211.20 m (Fig. 4A) is an organic-rich lime mudrock with abundant calcite micro-fossils (calcite-replaced sponge spicules?) and dense organic-rich layers with preserved calcispheres. The sample at 3210.73 m (Fig. 4B) is an organic-poor fractured lime mudrock. A calcite-healed fracture is noted. The sample at 3190.30 m (Fig. 4C) is very similar to the organic-rich lime mudrock of sample at 3211.20 m but contains abundant silt-sized quartz grains and no preserved fossil fragments. The sample at 3188.20 m (Fig. 4D) contains abundant silt-sized quartz grains and organic matter is rare.

The Ti-2 thin section samples from the Bay du Nord L-76z core are shown in Fig. 4E and F. The sample at 3123.17 m (Fig. 4E) is comprised of a mix of organic-poor muddy layers with abundant silt-sized quartz grains. The sample at 3098.42 m (Fig. 4F) has minor amounts of preserved organic matter, but silt and sand sized quartz grains are indicative of the deltaic sediment supply. Well preserved phosphatized fossil fragments are indicative of a more oxygenated environment.

In the Mizzen F-09 well, SWC thin section samples were selected from the Ti-1 and Ti-2 siltstone and mudstone intervals and representative photomicrographs are shown in Fig. 5. The sample at 3626.00 m (Fig. 5A) from the Ti-1 interval is a massive lime mudstone with abundant pyrite and well preserved fossil fragments and no visible OM is present. The SWC sample selected from the Ti-2 siltstone and mudstone intervals (Fig. 5B and C) show a laminated and bioturbated silty mudstone with silt-sized grains (mainly quartz) confined to the burrow-fill. This sample highlights a well preserved alginite fragment (Fig. 5C).

4.1.2. *Pyrolysis from the Ti-1 – Ti-2 siltstones and mudstones*

The pyrolysis data from the Ti-1 (Bay du Nord L-76z n = 8: Mizzen F-09 n = 0) and Ti-2 (Bay du Nord L-76z n = 6; Mizzen F-09 n = 7 drill cuttings only) siltstone and mudstone intervals show a wide range of values (Table 1). Pyrolysis results for the Ti-1 unit in the Bay du Nord L-76z show organic-rich sediments with TOC content ranging from 1.37 to 4.45 wt %. The HI values range from 30 to 264 mg HC/g TOC and the OI values range from 13 to 53 mg CO_2/g TOC showing OM type to be mainly a mix of Type II/III. Tmax ranges from 407 to 429 °C, reflecting the immature stage of thermal maturity. Pyrolysis results for the Ti-2 sequence show slightly higher TOC content ranging from 1.28 to 15.20 wt %. The HI values range from 45 to 504 mg HC/g and the OI values range from 4 to 47 mg CO_2/g TOC. The higher TOC and HI values reflect Type II OM. Tmax ranges from 410 to 423 °C also reflecting the low maturity stage of these sediments.

Seven drill cuttings samples were collected from the Ti-2 siltstone and mudstone section in Mizzen F-09. No samples were available from the Ti-1 unit. The TOC content results from the drill cuttings samples representing the Ti-2 intervals range from 3.15 to 5.12 wt %. The HI values range from 63 to 175 mg HC/g TOC. The OI values range from 11 to 30 mg CO_2/g TOC. Tmax values range from 402 to 426 °C. The HI and OI values are indicative of a mix of Type II/III OM.

The Bay du Nord L-76z and Mizzen F-09 pyrolysis results are plotted in Fig. 6A to F. HI vs. OI plots (pseudo van Krevelen diagram) show mixed Type II and Type III organic matter for both wells (Fig. 6A and B). The HI vs. Tmax plot shows immature Type II and Type III organic matter (Fig. 6C and D). The S2 vs. TOC plot for the Bay du Nord L-76z well (Fig. 6E) shows both the Ti-1 and Ti-2 units to contain good to excellent TOC (1.28–15.20 wt %) content, but the S2 values for most of the samples are mainly poor to fair (0.42–4.16 mg HC/g) The plot indicates that the OM is predominantly Type III and Type IV. However, one sample (Ti-2; 3354.7 m) plots as mixed Type II/III (S2 = 11.17 mg HC/g) and two samples (Ti-1) plot as Type II OM (S2 = 23.18 and 76.62 mg HC/g). These three samples were taken from just above and below

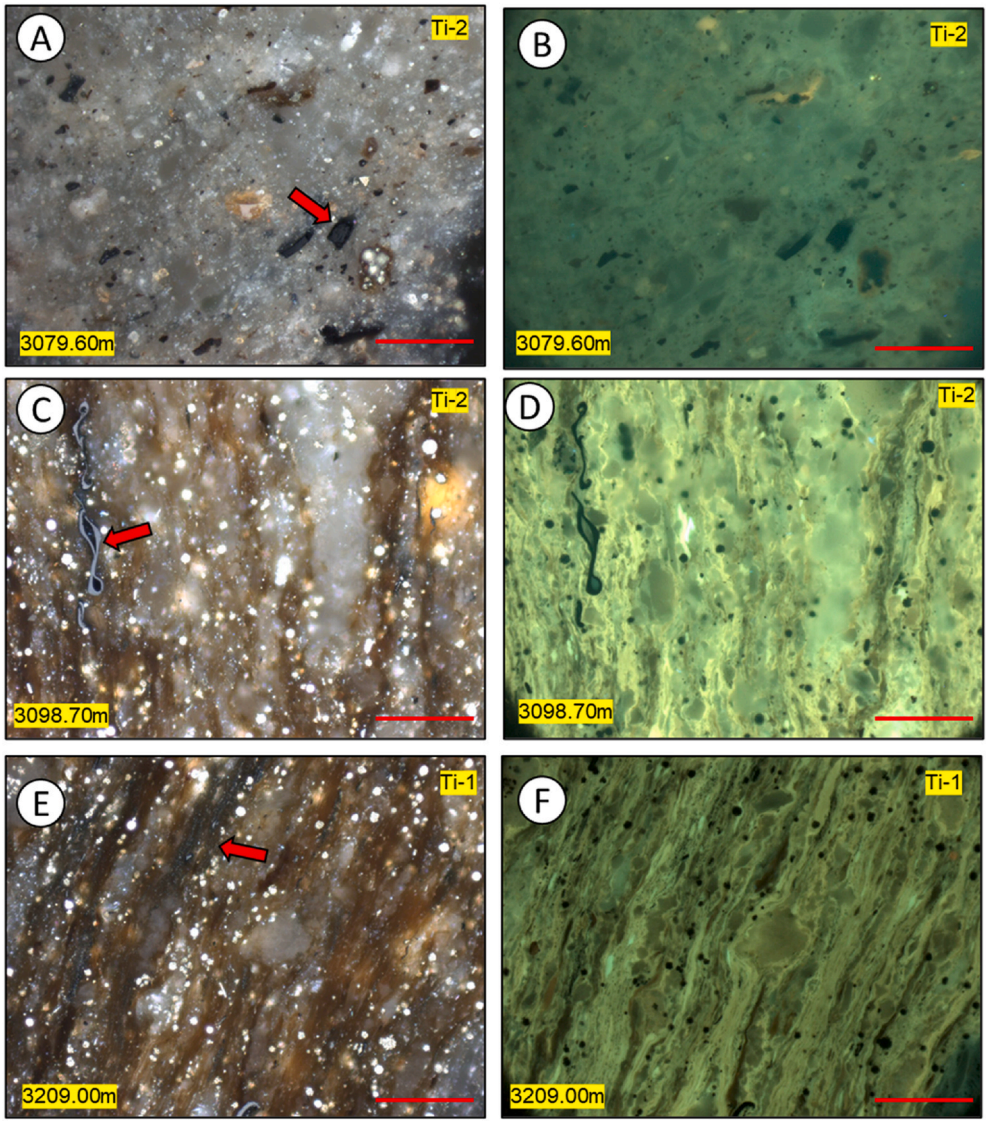

Fig. 7. Photomicrographs showing different types of organic particles from the Ti-1 and Ti-2 siltstones and mudstones in Bay du Nord L-76z. All photomicrographs are taken in under white light with oil immersion and a 50× objective was used. Red scale bar is 50 μm in length. A) Sample taken from the Ti-2 just under the Ti-3 subaerial unconformity in the deltaic deposits. Scattered organic fragments in an argillaceous matrix. An example of vitrinite is shown by red arrow. B) As in photo A but under fluorescence. C and E were taken at the Ti-1 and Ti-2 MFS and showing dark brown layers of lamalginite displaying condensed layers. A well preserved Zooclast is present in C (red arrow). Pyrite is abundant (black in fluorescence photos). Photos D and F are in fluorescence and display bright green fluorescence suggesting early oil window maturity. Some layers are bituminized as in E (arrow). These samples suggest a fully marine depositional environment. (For interpretation of the references to colour in this figure legend, the reader is referred to the Web version of this article.)

the Ti-1 MFS and at the MFS from the Ti-2 sequence (refer to Fig. 3). The S2 vs. TOC plot for the Ti-2 unit drill cuttings samples in the Mizzen F-09 well shows very good to excellent TOC content (3.15–5.12 wt %) and S2 values range fair to good (2.3–7.09 mg HC/g; Fig. 6F). The plot indicates the OM type is mainly Type II/II to Type III. However, none of the Mizzen F-09 drill cuttings samples represent the MFS as in Bay du Nord L-76z and were taken from the deltaic mudstone intervals only.

4.1.3. Organic petrology from the Ti-1 – Ti-2 siltstones and mudstones

Organic petrology for the Ti-1 (n = 1) and Ti-2 (n = 2) deltaic siltstone and mudstone units was only performed in the Bay du Nord L-76z well as no samples were available in these intervals for the Mizzen F-09 well. Point count results support the interpreted OM types from the pyrolysis data showing a mixture of allochthonous and autochthonous macerals including vitrinite, recycled vitrinite, inertinite, liptinite, and bituminite. Bituminite in this study in defined as degraded diagenetic solid bitumen, which is not a secondary maceral resulting from the thermal cracking of kerogen. Instead, it is derived from degradation of bituminite in the diagenesis stage (Ro < 0.5%; Sanei, 2020). The point count data can be viewed in Table 2.

The preserved populations of organic constituents include structured alginite and well preserved fluorescing lamalginite that make up 80–82% of the total maceral counts from the samples taken at the MFS in Ti-2 and Ti-1 sequence respectively. Other organic macerals include minor amounts of recycled vitrinite (1–5%), inertinite (5–10%), and degraded diagenetic solid bitumen (5–12%). Detrital silt-sized silicate fragments are almost non-existent and laminated lime mud content is high (20–30% $CaCO_3$ measured by pyrolysis; Table 1). Scattered framboidal pyrite is also present and is often in alignment with lamalginite algal material. The alginite macerals show bright yellow fluorescence suggesting low maturity (Ro < 0.5%; Sanei, 2020). One sample at 3079.60 m was selected to represent the terrigenous deltaic sediments but could not be point counted due to uneven polished surface. However, petrographic observations from this sample show no fluorescing liptinite macerals with minor amounts of vitrinite, recycled vitrinite, and inertinite. The mineral matter is high in this sample with abundant silt and sand-sized silicate grains indicating a more terrigenous sediment input. Organic maceral photomicrographs can be viewed in Fig. 7.

Tmax values from the Ti-1 pyrolysis data show 407 °C and 410–423 °C in Ti-2 unit. Thermal maturity based on converting the pyrolysis Tmax to $\%VRo_{equiv}$ (Jarvie, 2012) yields a $\%VRo_{equiv} = 0.17$ in the Ti-1 unit and a $\%VRo_{equiv} = 0.22$ to 0.45 in the Ti-2 unit. %VRo measured on one sample from the Ti-2 unit is 0.50%. These values are consistent with the immature window. Since %VRo cannot be accurately measured on fluorescing alginite and fluorescing lamalginite, thermal maturity measurements were taken on the degraded diagenetic solid

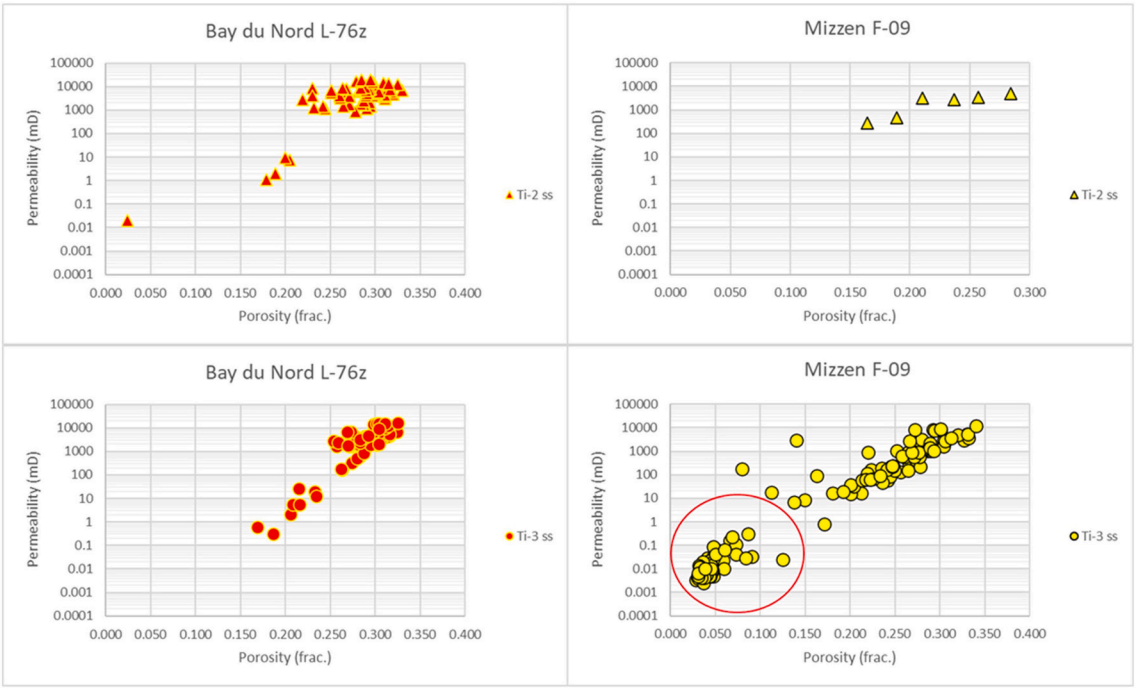

Fig. 8. Porosity and permeability results for Ti-3 and Ti-2 incised valley sandstones in Bay du Nord L-76z and Mizzen F-09. Red circle indicates samples that are calcite cemented resulting in poor reservoir quality in Mizzen F-09. (For interpretation of the references to colour in this figure legend, the reader is referred to the Web version of this article.)

bitumen (%Bro). %Bro values for the Ti-1 and Ti-2 units 0.26% and 0.30% respectively, consistent with the immature window. The measured thermal maturity of these samples is also consistent with the pyrolysis data. All of the reflectance data are reported in Table 2.

4.2. Ti-2 – Ti-3 incised valley sandstone core analysis, thin section petrography, pyrolysis, and organic petrology

4.2.1. Core analysis from Ti-2 and Ti-3 incised valley sandstones

The Bay du Nord L-76z core porosity values for the Ti-3 (n = 60) unit range from 16.9 to 32.5% (mean = 28.0%; ±3.4% SD) and permeabilities range from 0.31 to 16200.0 mD. Porosity values for the Ti-2 (n = 77) unit range from 2.4 to 33.0% (mean = 27.9%; ±4.3% SD) and permeabilities range from 0.0197 to 18800.0 mD. In Mizzen F-09 core porosities for the Ti-3 unit (n = 134) range from 2.8 to 34.0% (mean = 16.5%; ±11.0% SD) and permeabilities range from 0.001 to 12107.4 mD. The Ti-2 (n = 14 SWC only) porosities range from 0.3 to 28.4% (mean = 13.7% ± 9.0% SD) and permeability range from 0.0007 to 5000.0 mD. The Mizzen F-09 core data shows that the mean porosity values are lower with a higher standard deviation than in the Bay du Nord L-76z core porosity values. This is due an abundance of pore-filling calcite cement in Mizzen F-09 (3.0–31.0%) that severely reduces reservoir quality (Fig. 8). All porosity and permeability data can be viewed in Table 3.

4.2.2. Thin section petrography from Ti-2 and Ti-3 incised valley sandstones

In the Bay du Nord L-76z well the samples range from litharenites to sublitharenites to feldspathic litharenites based on Folk's (1980) classification scheme. Four samples representing the Ti-3 incised valley sandstones are feldspathic litharenites (10–16% feldspars). Two samples near the top of the Ti-2 incised valley sandstones are feldspathic litharenites and the rest of the samples range litharenites to sublitharenites (Fig. 9). Visual grain sorting is poor to well, with some samples exhibiting a bimodal sorting pattern. The Ti-3 sands average grain size is very fine (upper) to upper fine. The Ti-2 sands average lower fine to upper medium and range from silt to locally conglomeratic. Samples are mainly structureless but range from slight grain alignment to cross-laminated. Laminations are defined by changes in grain size. The effects of mechanical and chemical compaction are very low. Most of the grains are tangential to point contact and some grains appear to float in the blue-dyed epoxy resin. The occasional presence of sutured contacts is also present in some samples. Representative photomicrographs of the Ti-2 and Ti-3 incised valley sandstones are shown in Fig. 10. All thin section point count data is shown in Table 4.

In the Bay du Nord L-76z well the Ti-2 and Ti-3 incised valley sandstones framework grains include monocrystalline quartz as the main detrital grain with lesser amounts of polycrystalline quartz. Potassium feldspars are generally slightly more abundant than plagioclase. Lithic rock fragments include allochthonous limestone fragments, volcanic and metamorphic fragments, mudstone fragments, silt/sand fragments, a minor amount of dolostone fragments, micas, dispersed organic matter sometimes occur along laminations, and trace heavy minerals (zircon, rutile, and tourmaline). Calcareous shell fragments, ooids, and phosphatic fragments are occasionally present and well preserved suggesting the sand source was marine or from erosion of older sediment. Trace amounts of detrital illitic clay is present as pore-lining and/or grain-coating.

Authigenic minerals include minor amounts of quartz overgrowths on monocrystalline quartz grains that were likely inherited from an older sediment. Feldspar overgrowths, calcite and ferroan calcite, dolomite and ferroan dolomite, pyrite, siderite, kaolinite, illite, and chlorite are variably present in minor to trace amounts. Ferroan dolomite is the most abundant cement type in Ti-2 (27%) at depth 3168.85 m. Excellent secondary porosity after cement dissolution is well developed in both the Ti-2 and Ti-3 units. Thin section photomicrographs from Bay du Nord L-76z showing framework and authigenic mineralogy can be viewed in Fig. 10.

In the Mizzen F-09 well there are two well developed incised valley units within the Ti-2 sequence (refer to Fig. 3). The Ti-2 lower unit in Mizzen F-09 consists of moderately well to well sorted sublitharenites. Grain size ranges from upper fine to upper medium. Monocrystalline

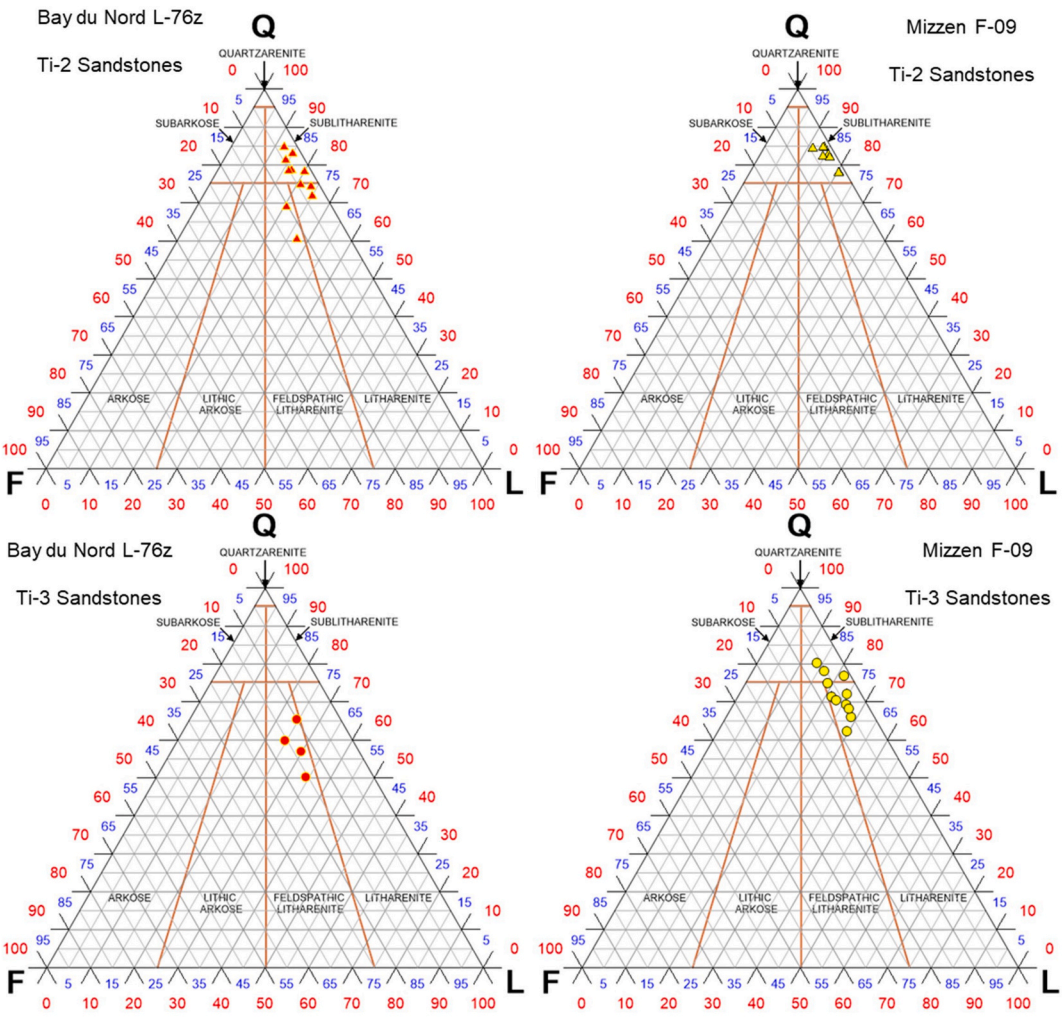

Fig. 9. Folk ternary diagrams showing rock type classification according to Folk (1980) from Bay du Nord L-76z and Mizzen F-09 Ti-3 and Ti-2 sandstones.

quartz dominates the framework mineralogy with very minor feldspar. Lithic fragments consist of chert, siltstone, and schistose metamorphic. Some lithic fragments are partially dissolved. Rare quartz overgrowths are present with minor amounts of calcite and dolomite. Dolomite cement is most abundant in the basal part of the unit. Secondary porosity after cement dissolution is abundant (>25%).

The Ti-2 upper unit in Mizzen F-09 consist of structureless to faintly laminated poorly to moderately to locally bimodal sorted sublitharenites. Grain size ranges from lower medium to lower coarse with grain size slightly increasing with depth. Monocrystalline quartz is the dominant detrital mineral with very few feldspars. Lithic fragments increase with depth but are a minor detrital constituent. Lithic fragments include allochthonous carbonate, well preserved fossils, siltstone/mudstone, and metamorphic. Authigenic minerals include minor quartz overgrowths and calcite cement. Good secondary porosity after cement dissolution is preserved at the top of the unit. However, calcite cement increases towards the base and is occluding almost all of the porosity.

The Ti - 3 sandstone unit (n = 11) in Mizzen F-09 is the only cored interval in the well and is the primary reservoir target. Based on Folk's (1980) classification the samples range litharenites to sublitharenites that are marginally feldspathic (1.0–7.0%; Fig. 9). Grain sizes range from lower fine to lower coarse to locally conglomeratic near the base of the core. Samples are mainly structureless to faintly laminated with local calcite-healed fractures. Monocrystalline quartz is the dominant detrital mineral with minor to common feldspars. Lithic fragments include allochthonous carbonate and oolitic grains, well preserved fossils, siltstone/mudstone, and metamorphic. Authigenic minerals include minor inherited quartz overgrowth and calcite cement is abundant. Calcite cement is most abundant near the base of this unit. Calcite cement is stained pink in almost all samples indicating low iron content and occurs as large poikilotopic crystals. Minor amounts of pyrite and authigenic kaolinite is also present. Several intervals are not cemented and have well preserved porosity, but calcite cement is pervasive in this unit. All representative photomicrographs are shown in Fig. 11.

4.2.3. *Pyrolysis of interlaminated mudstone intervals within the Ti-2 and Ti-3 incised valley fill sandstones*

The interlaminated mudstones within the Ti-2 and Ti-3 in the Bay du Nord L-76z incised valley sandstone units show good preservation of organic material (TOC = 2.29 to 6.77 wt %). HI values range from 73 to 157 mg HC/g TOC. OI values range from 5 to 27 mg CO_2/g TOC. Tmax values range from 411 to 419 °C (Table 1). The pseudo van Krevelen diagram shows mixed Type II/III OM for both units. The HI vs. Tmax plot shows mainly a mix of Type II/III OM with very low maturity. The S2 vs. TOC plot shows TOC preservation to be very good to excellent (2.29–6.77 wt %), but most of the samples a have poor to fair S2 values (1.9–5.08 mg HC/g). One sample from the Ti-2 unit (3161.47 m) has excellent TOC (6.77 wt %) content and very good S2 (10.67 mg HC/g). All samples plot within the Type III range on the S2 vs. TOC plot (Fig. 12).

Only the interlaminated mudstones within the Ti-3 sandstone unit were analyzed in the Mizzen F-09 well. TOC values range from 1.63 to

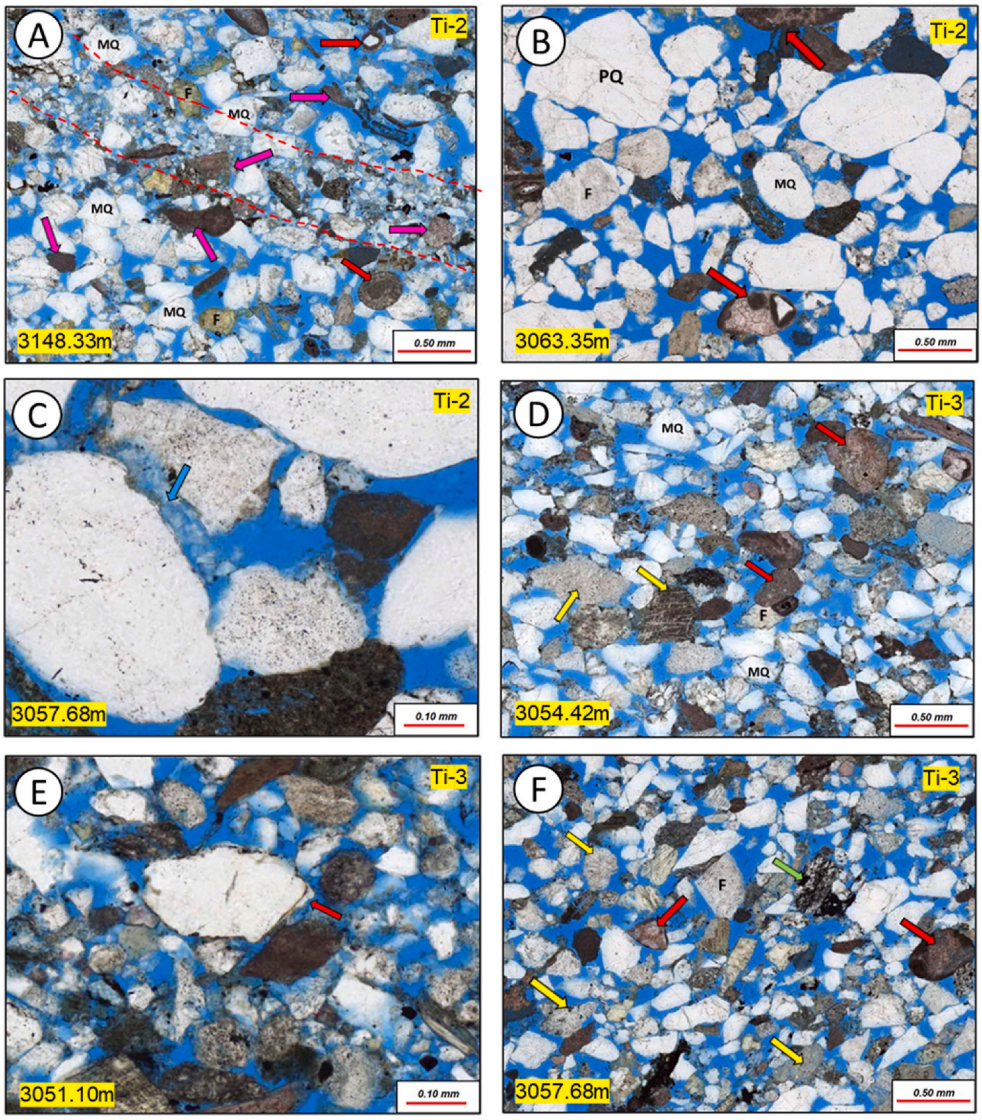

Fig. 10. Representative thin section photomicrographs of the Ti-2 and Ti-3 incised valley sandstones in Bay du Nord L-76z showing framework and authigenic mineralogy. A) Vaguely laminated, moderately sorted, upper very fine grained feldspathic litharenite. Red dashed line outlines lamination of finer grained detrital grains. Monocrystalline quartz (MQ) is the dominant framework grain. Potassium feldspar (F) are stained yellow. Limestone rock fragments are abundant (pink arrow). Oolitic grains are also present (red arrows). B) Upper medium grained sublitharenite. Abundant monocrystalline quartz (MQ) with minor polycrystalline quartz (PQ) and feldspar (F). Lithic fragments include abundant reworked limestone grains (red arrows). C) A closer view of showing a minor amount of kaolinite (blue arrow. D) Upper fine grained feldspathic litharenite with abundant monocrystalline quartz (MQ) grains and feldspar (F). Limestone rock fragments (red arrows) and volcanic rock fragment (yellow arrows) are the dominant lithic grains. E) Close view showing quartz overgrowths (red arrow). Rare quartz overgowths are discontinuous and broken suggesting they were inherited from a previous sandstone. F) Feldspar (F), volcanic rock fragments (yellow arrow), metamorphic rock fragments (green arrow), and limestone rock fragments (red arrows) make up a large portion of the lithic grains. Note excellent preserved secondary porosity (blue dye epoxy). (For interpretation of the references to colour in this figure legend, the reader is referred to the Web version of this article.)

27.92 wt %. The HI values range from 47 to 412 mg HC/g TOC. OI values range from 3 to 22 mg CO_2/g TOC. Tmax values range from 401 to 426 °C (Table 1). The pseudo van Krevelen diagram shows mixed Type II/III OM. The HI vs. Tmax plot shows mainly a mix of Type II/III OM with very low maturity. The S2 vs. TOC plot shows TOC content to be good to excellent (1.63–27.92 wt %), but most of the samples have poor to fair S2 values (0.8–7.32 mg HC/g). Two samples from this unit (3376.50 and 3382.05 m) have excellent TOC (17.60 and 27.92 wt %) content and very good S2 (56.18–113.59 mg HC/g). Most of the samples plot within the Type III range with the exception of two samples that plot in the Type II range on the S2 vs. TOC plot (Fig. 12).

4.2.4. Organic petrology of interlaminated mudstone intervals within the Ti-2 and Ti-3 sandstones

Optical microscopy of the organic matter in the Bay du Nord L-76z well shows the Ti-2 incised valley sandstone sample (n = 1) to have well preserved vitrinite fragments as well as reworked vitrinite, degraded diagenetic solid bitumen, and minor inertinite. The Ti-3 incised valley sandstone sample (n = 1) is nearly all non-fluorescencing liptinite, degraded diagenetic solid bitumen, and minor inertinite. Photomicrographs of the organic petrology can be viewed in Fig. 13.

The pyrolysis Tmax show these samples to be in the immature window (Tmax = 411–417 °C). The reflectance value from the Ti-3 sample is 0.49%. The $\%VRo_{equiv}$ (Jarvie, 2012) is 0.35%. The average reflectance values measured on the degraded diagenetic solid bitumen in the Ti-2 sample is 0.23%. No true vitrinite was identified in this sample. The estimated $\%VRo_{equiv}$ from pyrolysis Tmax (0.24%) is in excellent agreement with the reflectance values measured on degraded diagenetic solid bitumen (%Bro = 0.23%). All reflectance data can be viewed in Table 2.

Three organic petrology samples were selected from the interbedded mudstone intervals within the Ti-3 incised valley sandstone unit from the Mizzen F-09 well. The sample at 3341.65 m could not be point counted due to the uneven polished surface of the sample pellet. Microscopic observations revealed an abundance of recycled vitrinite and degraded diagenetic solid bitumen. Only a minor amount of scattered fluorescent alginite is present. Silty mudstone mineral mass is abundant suggesting a terrigenous sediment source. The sample at 3382.05 m shows an abundance (27%) of bright green fluorescing structured alginite as lamalginite to be present in a very thin lime mudstone bed. Degraded diagenetic solid bitumen is abundant (60%) in this sample and minor amounts of vitrinite (10%) and inertinite (3%) are also present. The sample at 3387.30 m shows minor amounts (4%) of bright green-fluorescent alginite as well as very minor amounts of vitrinite (10%) and inertinite (2%). Degraded diagenetic solid bitumen is abundant (84%). All representative photomicrographs are in Fig. 14.

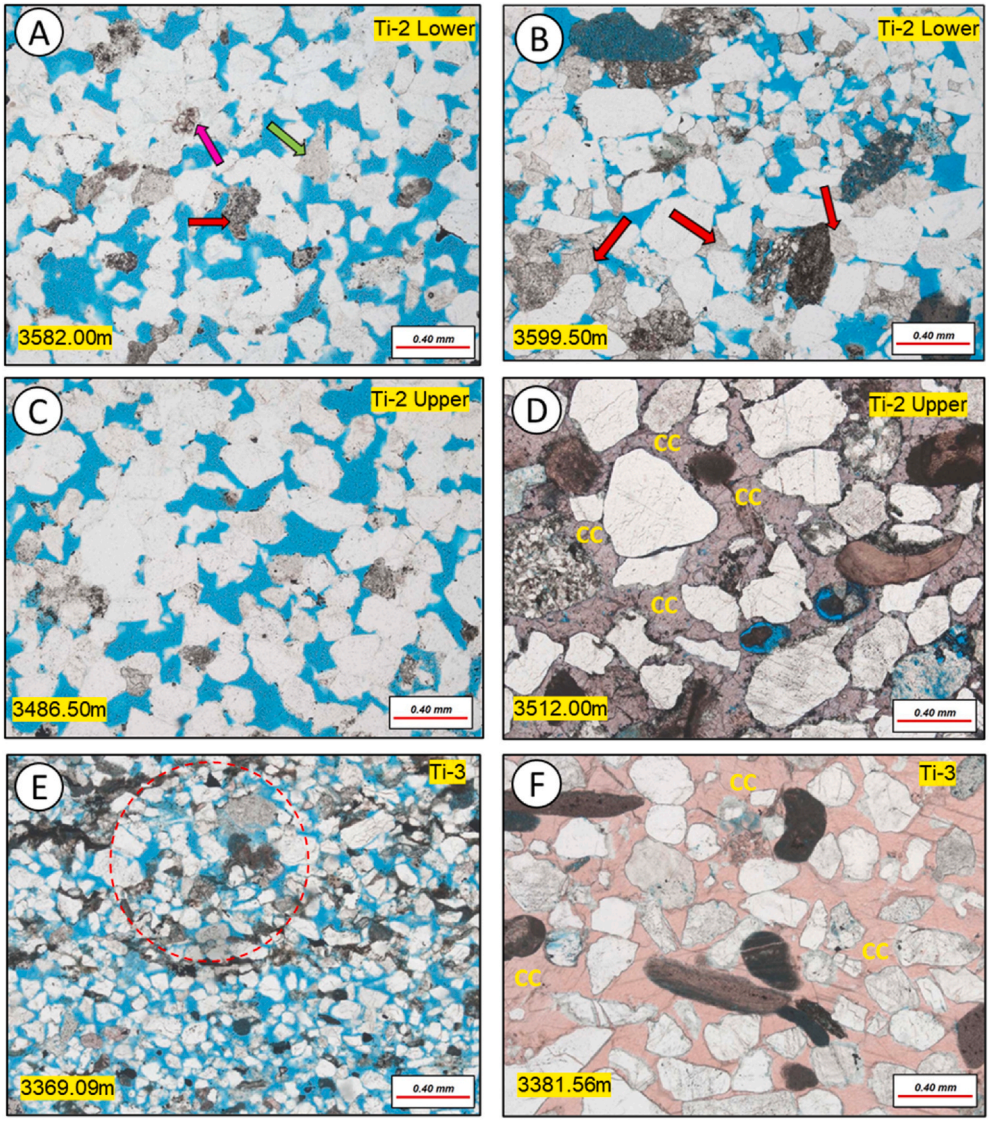

Fig. 11. Representative thin section photomicrographs of the Ti-2 (lower and upper) and Ti-3 incised valley sandstones in Mizzen F-09 showing framework and authigenic mineralogy. A) Moderately well to well sorted sublitharenite. Monocrystalline quartz (white grains) dominates the framework mineralogy with very minor feldspar. Lithic fragments consist of minor amounts of chert (green arrow), siltstone (red arrow), and schistose metamorphic (pink arrow). B) Patchy dolomite cement is most abundant in the base of the unit (red arrow). Excellent secondary porosity is preserved in the Ti-2 units (blue dyed epoxy). C) Similar to samples in A. D) The base of the Ti-2 Upper unit is pervasively cemented with slightly ferroan calcite cement (cc). E) Lower fine grained litharenite that is marginally feldspathic. Grain size varies in this unit from lower fine to lower coarse. Sample appears to be bioturbated (red circle). F) Non-ferroan calcite cement (cc) increases toward the base of the Ti-3 unit and becomes pervasive. (For interpretation of the references to colour in this figure legend, the reader is referred to the Web version of this article.)

%BRo measured on degraded diagenetic solid bitumen ranges from 0.19 to 0.45%. The $\%VRo_{equiv}$ derived from pyrolysis Tmax (Jarvie, 2012) ranges from 0.15 to 0.45%. This is in excellent agreement with the measured reflectance data and support the thermal maturity of these sediments to be in the immature window. Reflectance data can be viewed in Table 2.

4.3. Cathodoluminescence petrography

Cathodoluminescence (CL) petrography can be useful to examine calcite cement as it can show distinctive zonation of crystal growth cause by different phases of diagenesis (Sommer, 1972). Mn^{2+} is the element that is the activator of luminescence and Fe^{2+} is the element responsible for quenching the luminescence (Sommer, 1972). The lower the Fe/Mn the brighter the luminescence (bright red to orange) and the opposite (dull to nonexistent) form higher Fe/Mn values (Machel, 1985). The amount of luminescence or quenching can be used to suggest the composition of the diagenetic fluids that precipitated the cements (Frank et al., 1982; Blamey et al., 2014). In this study, all of the poikilotopic pore-filling cements, ferroan cements, and dolomite cements show an evenly distributed dull to non-existent luminescence in both wells. Only a few scattered detrital limestone fragments show bright orange luminescence. No concentric zoned mineral growth phases were detected. This suggests that the calcite cements precipitated from a Fe-rich homogeneous fluid composition in a single event. CL photomicrographs can be viewed in Fig. 15.

4.4. Paragenetic sequence of diagenetic events

Diagenesis can be described as the chemical and mechanical processes that are involved during sediment burial (Bjorlykke and Jahren, 2012). Here we use the terms to describe diagenetic events suggested by Horsfield and Rullkötter (1994) that take thermal maturity into account: i) diagenesis (%VRo= <0.5; burial temperatures up to 50–60 °C), ii) catagenesis (%VRo = 0.5 to 2.0; burial temperatures from 60 to 140–150 °C) and iii) metagenesis (%VRo = >2.0; temperatures >140–150 °C). Burial temperature data collected by proprietary oil and gas industry basin modelers show that the Flemish Pass Basin likely never got hotter than 110 °C at the Tithonian/Kimmeridgian contact (Wong, 2021; Pers Comm). Therefore, the late stage of catagenesis and metagenesis stage never affected these Late Tithonian sediments.

Detailed thin section petrographic analysis reveals the relative timing of major diagenetic events based mainly on cross-cutting relationships and simple cement stratigraphy relative to framework grains and/or other diagenetic minerals. Based on the thermal maturity results from this study these sediments have a maximum %VRo of 0.50%. The

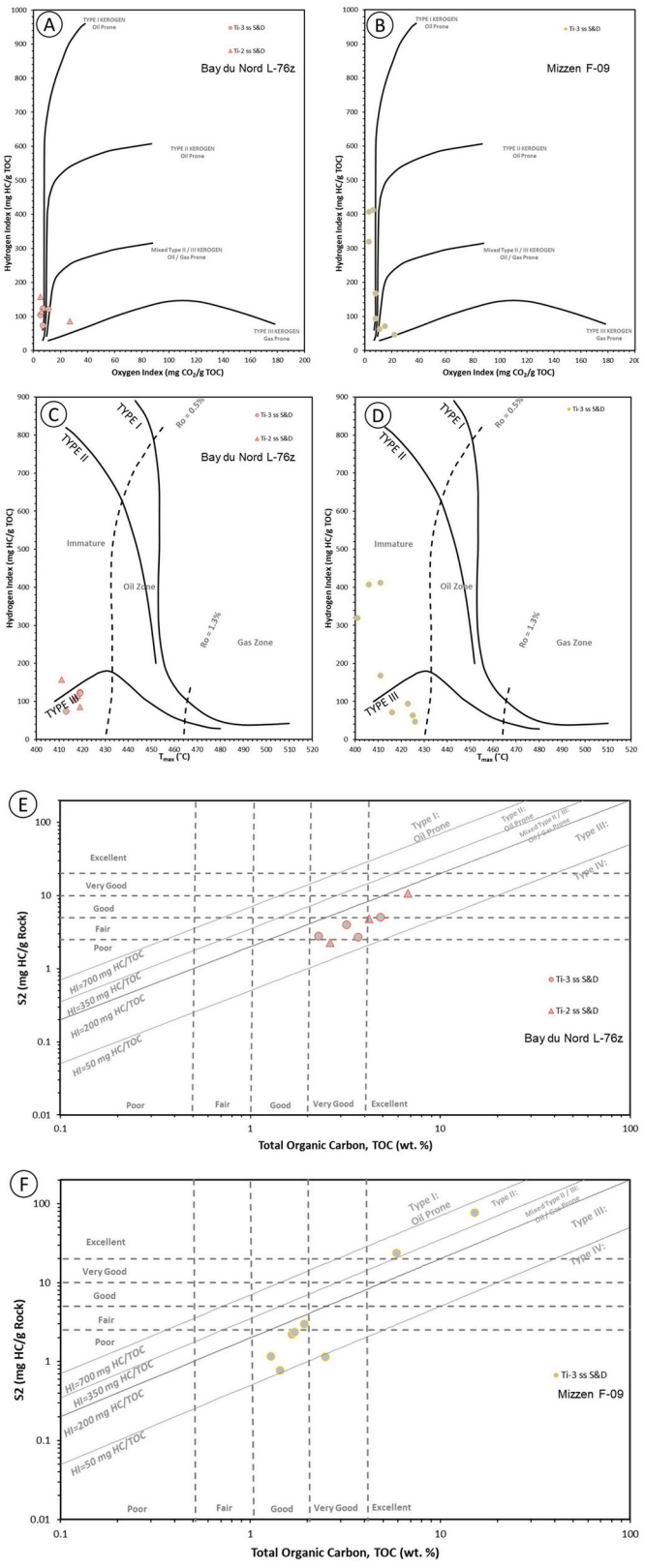

Fig. 12. Pyrolysis data plots for Bay du Nord L-76z Ti-2 and Ti-3 and Mizzen F-09 Ti-3 incised valley sandstone interlaminated organic matter.

immature OM thermal maturity suggests the diagenetic events are constrained to the late diagenesis to early catagenesis stage of approximately 60 °C. From these observations a generalized paragenetic sequence was constructed for the Ti-2 and Ti-3 incised sandstones (Fig. 16). Although, both Mizzen F-09 and Bay du Nord L-76z appear to have undergone similar diagenetic processes, the Mizzen F-09 well contains a greater amount of preserved pore-occluding calcite cement than in Bay du Nord L-76z significantly reducing the reservoir quality in Mizzen F-09, especially in the Ti-3 sandstone interval. However, the Ti-2 units in Mizzen F-09 have undergone almost complete dissolution of calcite cement and the reservoir quality is better preserved. The paragenetic sequence is explained below in order of occurrence. Thin section photomicrographs showing examples of diagenetic mineralogy can be viewed in Fig. 17.

4.4.1. Digenesis Stage (%VRo ≤0.50; low burial temperature from the sediment/water interface up to 50–60 °C)

4.4.1.1. Compaction (mechanical and chemical). Mechanical compaction takes place immediately after burial in most sediments and generally continues throughout the whole burial history of the rock unit (Bjørlykke et al., 2017). However, mechanical compaction appears to have very little affect on these sandstones. This is evident by the amount of floating grains and grains that are in point-to-point contact either in cemented or non-cemented zones. Ductile rock fragments including scattered organic matter, silt/mudstone, and schistose metamorphic all show minor grain deformation reflecting early stage compaction with grain rotation and adjustment to the boundaries of adjacent ridged grains (Fig. 17A). Very few grains do appear to show early signs of chemical compaction evident as minor pressure solution seams at grain to grain contacts (Fig. 17B).

4.4.1.2. Pyrite. Pyrite occurs as cubic crystals that have partially replaced some fossil fragments, carbonate rock fragments, and partial replacement of ooids (Fig. 17C). Pyrite predates the calcite cementation.

4.4.1.3. Dolomite. Minor amounts of early dolomite rhombs and cement are present. The rhombs are locally observed to grow into quartz cement (Fig. 17D), which indicates the dolomite post-dates quartz overgrowths as almost all quartz overgrowths are presumed to be inherited from the erosion of an older sediment. Individual dolomite rhombs are often ferroan and in rare cases show a non-ferroan core with a ferroan rim that may be the result of temporal fluctuations in iron concentrations of the pore water (Caplan and Moslow, 1998; Vandeginste and John, 2012). It is likely that at the time of deposition seawater actively mixed with fresh water that resulted in the dolomitization of aragonite and/or early calcite (Teal et al., 2000).

4.4.1.4. Siderite. Siderite is rare, but when present show small lozenge shaped euhedral crystals that likely replace sedimentary mudstone fragments. The siderite pre-dates calcite cementation as it can be observed sandwiched between quartz – quartz contacts (Fig. 17E).

4.4.1.5. Feldspar dissolution. Feldspars are often partially to almost completely dissolved and some are preserved only as uncompacted grain ghosts. Many feldspars have been subsequently filled with slightly ferroan to non-ferroan calcite cement (Fig. 17F) indicating early dissolution from meteoric water before calcite cementation.

4.4.1.6. Quartz overgrowths. A minor amount of authigenic quartz appears as syntaxial overgrowths on monocrystalline quartz grains. Quartz overgrowths are almost non-existent in heavily calcite cemented zones, but where rarely preserved the quartz cement appear to predate the calcite cement and generally appear discontinuous and have corroded and/or abraded edges. This suggests they have been inherited from an older sediment and not formed *in situ*. In very rare occurrences quartz overgrowths in highly porous zones have euhedral crystal faces that must have formed *in situ* (e.g., Fig. 18D). Feldspar dissolution can provide a source of silica for quartz overgrowths, therefore it is possible that

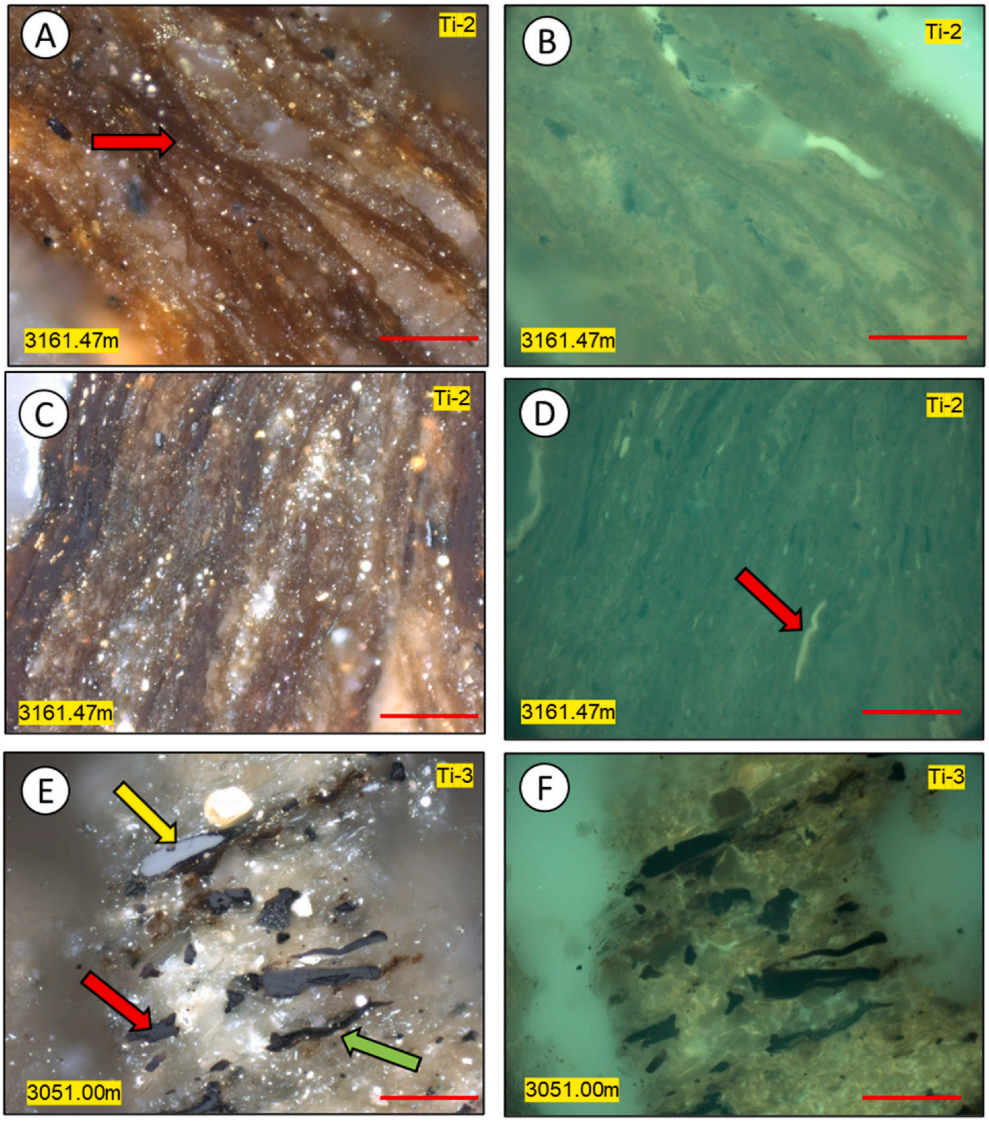

Fig. 13. Photomicrographs showing different types of organic particles from the Ti-2 and Ti-3 incised valley sandstone interlaminated organic matter in Bay du Nord L-76z. All photomicrographs are taken in under white light with oil immersion and a 50× objective was used. Red scale bar is 50 μm in length. A) – D) Dark brown condensed layers of lamalginite (red arrow). These samples are not fluorescing. Only one small particle in photo D is fluorescing (red arrow). E) Sample taken just above the Ti-3 incised valley fill and may be more representative of deltaic depositional environment. This sample shows well preserved vitrinite (red arrow), bituminite (green arrow), and inertinite (yellow arrow). (For interpretation of the references to colour in this figure legend, the reader is referred to the Web version of this article.)

a minor amount of early quartz overgrowths formed just after feldspar dissolution and before calcite cement formation (Huan et al., 2021). Quartz overgrowths can form in the catagenesis stage from temperature ranging 90–100 °C (Haile et al., 2020). This is further evidence that most quartz overgrowths did not form *in situ* as the thermal maturity data from this study suggests the sediments never got the hotter than approximately 60 °C.

4.4.1.7. Kaolinite. A minor amount of authigenic kaolinite was observed occurring as scattered booklets in non-cemented pores (Fig. 17G). Partially leached feldspar grains encased in calcite cement suggests an early phase of feldspar dissolution by meteoric water since kaolinite forms at the expense of potassium feldspar (Yuan et al., 2019).

4.4.1.8. Calcite cement. Calcite is the dominant authigenic mineral controlling reservoir quality in the Ti-3 and Ti-2 incised valley sandstones (up to 30%). It occurs mainly as pore-filling poikilotopic pervasive cement (Fig. 17H). It also occurs as early fibrous euhedral crystals formed on some limestone fragments and as a replacement mineral (Fig. 17I). Calcite cement has a greater abundance in the Mizzen F-09 well, especially in the Ti-3 interval, than the Bay du Nord L-76z well and mainly occurs in the coarser grained sands near the base of the interval. The majority of the calcite in non-ferroan (stained red in thin section) to slightly ferroan (stain has a slightly purple hue in thin section; Fig. 17J), but ferroan calcite (dark blue in thin section) is also present (Fig. 17K). These variable iron-rich cements do not show any differences in luminescence in CL petrography indicating a homogeneous cement phase. The loosely packed framework grains are encased in the cement giving the grains a floating appearance indicating early precipitation prior to and halting mechanical compaction. Calcite twinning planes observed under crossed polarized light appear to be continuous on either side of the framework grains suggesting the cement consumed the grains before any other diagenetic events occurred (Blamey et al., 2014; Xiong et al., 2016). It is likely that the original sand sediment contained a larger amount of shell and limestone fragments than is presently preserved. Aragonite and Mg-calcite allochems are highly unstable (Loucks and Patty, 2017), and the break down of these unstable allochems were a likely source of calcium for the calcite cement. The calcite cemented zones in Mizzen F-09 have been described as large concretions (often larger than core diameter) that have nucleated from calcite allochems that were eroded from the sediment source and redeposited in the Tithonian incised valley sandstone units (Haynes et al., 2014). Hesse and Abid (1998) in their study of similar calcite cemented sandstones in the Hibernia offshore Newfoundland area noted that because there are abundant preserved limestone and fossil fragments in non-cemented porous sandstones that other sources of calcite are possible such as

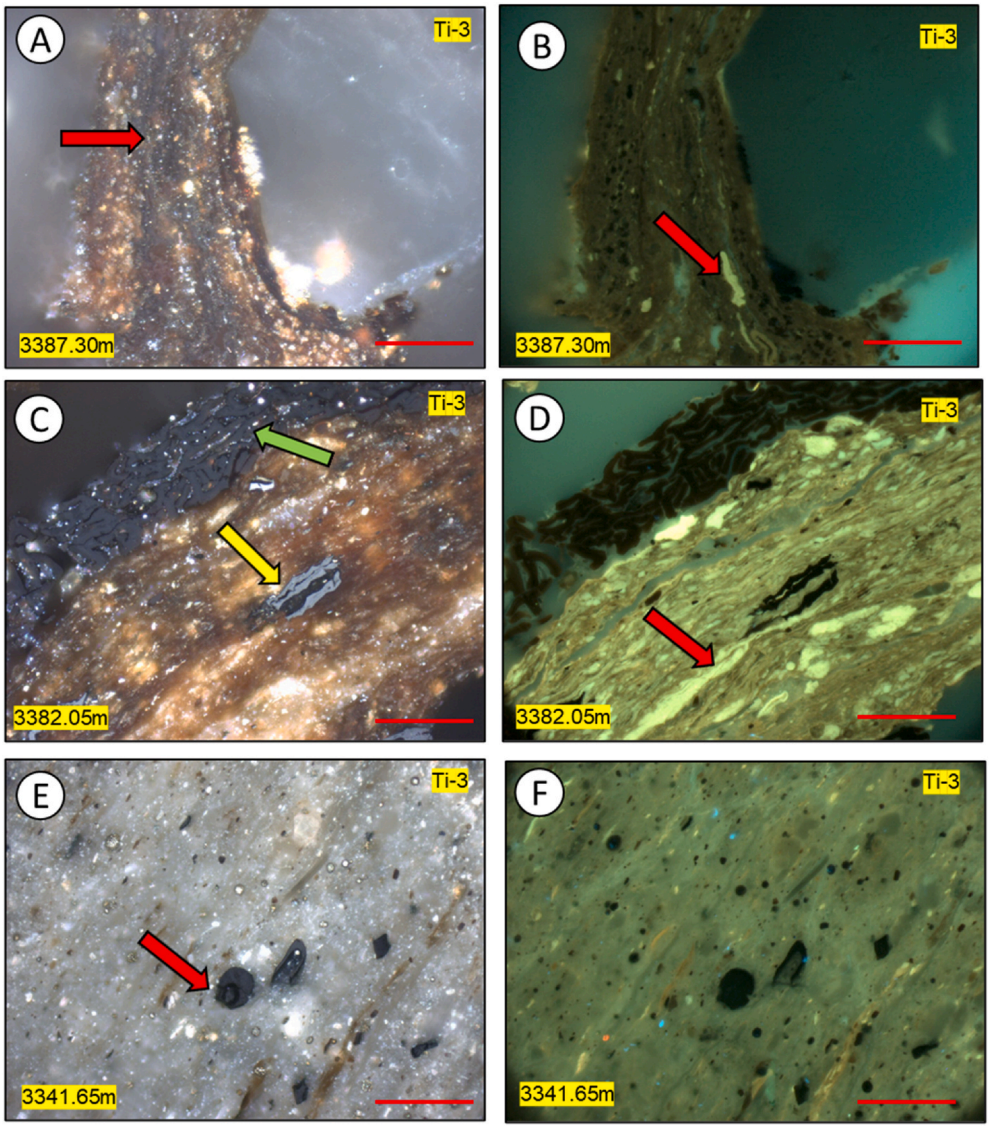

Fig. 14. Photomicrographs showing different types of organic particles from the Ti-3 incised valley sandstone interlaminated organic matter in Mizzen F-09. All photomicrographs are taken in under white light with oil immersion and a 50× objective was used. Red scale bar is 50 μm in length. A) Dark brown condensed layers of lamalginite that have been bituminized (red arrow). B) A minor amount of scattered alginite is fluorescing (red arrow) C) A mixture of dark brown layers of lamalginite and well preserved bituminite (green arrow). Minor highly reflecting Zooclasts are also present (yellow arrow). D) Sample field of view as in C but showing bright green fluorescing lamalginite (red arrow). These samples are indicative of a marine environment and were taken in the TST of the incised valley. E) Scattered vitrinite (red arrow) and minor alginite in a silty argillaceous matrix. This sample is suggestive of a deltaic environment and was taken just above the incised valley top. F) Same photo as E but under fluorescence. Very minor fluorescence is visible. (For interpretation of the references to colour in this figure legend, the reader is referred to the Web version of this article.)

percolating meteoric water that is saturated with respect to calcite. Reported $\delta^{18}O$ values suggest that the fluids that precipitated the calcite cement in the Flemish Pass area may have been a mixture of meteoric and marine water (Hesse and Abid, 1998; Xiong et al., 2016). Stable isotope data on dolomite and calcite cements in the neighbouring Jeanne d' Arc Basin show the carbonate cements are a mix of meteoric and marine water and may have precipitated at temperatures from 25 to 35 °C (Olanipekun and Azmy, 2021). Similar results have been reported by Xiong et al. (2016) who suggested a calcite precipitation temperature of 25–40 °C based on their stable isotope data from the Ti-3 incised valley sandstone in Mizzen F-09. This is consistent with precipitation in the early diagenesis stage.

4.4.1.9. Dissolution. To understand the presence of secondary porosity by dissolution it is critical to petrographically observe the contacts of grain to cement boundaries in the pervasively cemented sandstones and compare those observation to the non-cemented zones. The fluids that precipitate the carbonate cement are alkaline and are corrosive to siliceous framework grains (May, 1980). These petrographically observable textures include grain embayment where carbonate cement has penetrated into a siliceous framework grain by partially replacing the grain (Fig. 18A), pits and notches that often show the rhombohedral shape of the penetrating carbonate cement in the framework grain, and depressions from corrosion where the cement has partially or completely removed the quartz overgrowths on framework monocrystalline quartz grains (Fig. 18B). These textures are often preserved on the grain to pore boundaries in the porous zones and indicate a precursor cement was present but leached away (Fig. 18B). In some samples partially leached patches of carbonate cement still remain only moderately reducing reservoir quality (Fig. 18B). Another indication of secondary porosity after carbonate cement dissolution is the loose grain packing and the framework grains appear to "float" in the blue dyed epoxy resin injected during thin section preparation that represents the porosity (Fig. 18C). This suggests that mechanical compaction had little affect on these sandstones due to early precipitation of calcite cement that halts any further compaction of the sediment. Excellent secondary porosity is present where the carbonate cement has been dissolved. If the calcite cement were not an early diagenetic event, the effects of mechanical compaction would have severely reduced reservoir quality of these sandstone given the depth of burial of 2–3 km. Also, given the high quartz content in these sandstones, the effects of chemical compaction by the close packing of grains would have fused quartz grains together caused by pressure solution reducing the reservoir quality by formation of abundant quartz overgrowths in the open pore space (Dickinson, 1985; Surdam et al., 1989; Stück et al., 2013).

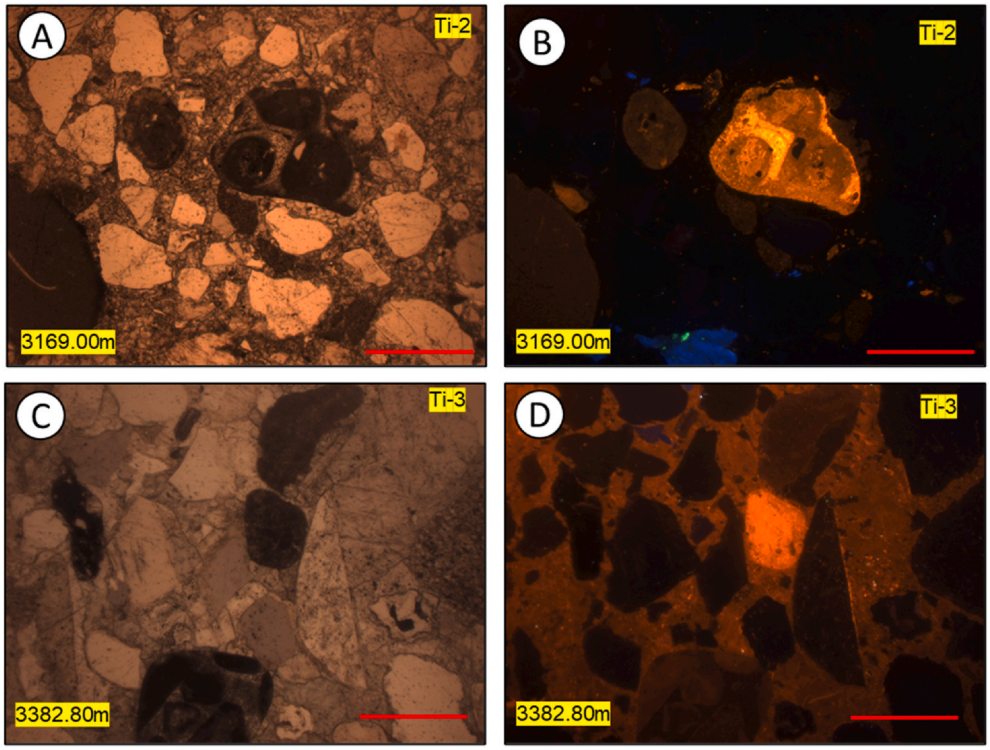

Fig. 15. Cathodoluminescence (CL) photomicrographs. Red scale bar is 0.5 mm. A) Plain light view of Ti-2 incised valley cemented sandstone sample from Bay du Nord L-76z. B) CL view showing only allochthonous limestone fragments luminesce. The cements show no luminescence at all suggesting there is no cement zonation in these samples. C) Plain light view of Ti-3 incised valley cemented sandstone sample from Mizzen F-09. D) CL view showing no cement luminescence. Only one allochthonous limestone fragment show luminescence. (For interpretation of the references to colour in this figure legend, the reader is referred to the Web version of this article.)

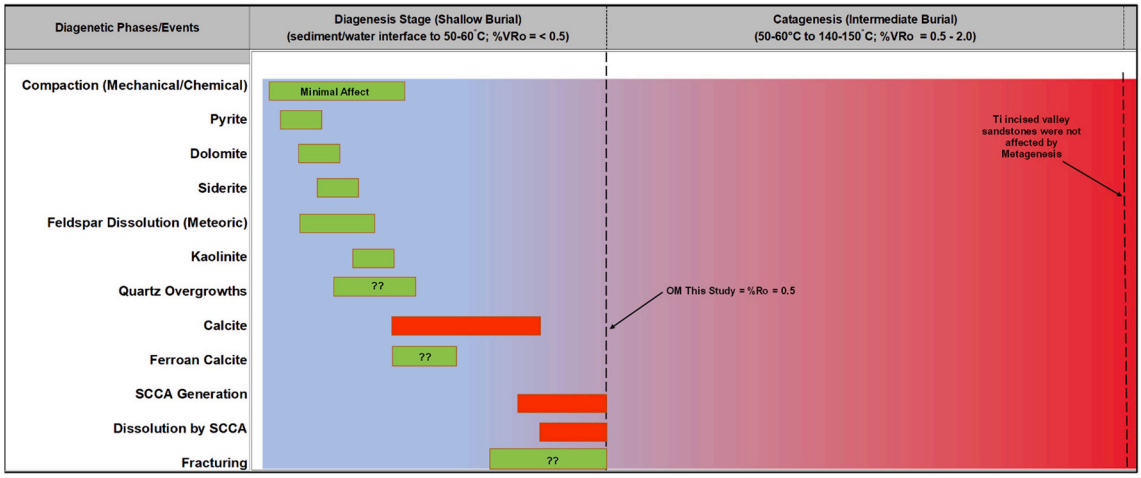

Fig. 16. Diagenetic sequence of events for Ti incised valley sandstones. A) Shows all diagenetic events in order of occurrence up to a maximum burial temperature of approximately 60 °C. Green bars indicate minor diagenetic events and red indicate major events. (For interpretation of the references to colour in this figure legend, the reader is referred to the Web version of this article.)

4.4.1.10. Fracturing. In the samples chosen for this study very few fractures were identified. Where present they are calcite and/or ferroan calcite filled. The fractures were likely the last event in the paragenetic sequence to take place as they crosscut all of the sediment and cement (Fig. 18E).

4.4.1.11. Intergranular volume. Intergranular volume (IGV) is the sum of intergranular pore space, intergranular cement, and matrix (Houseknecht, 1987; Paxton et al., 2002). Matrix can be defined as muds and silt particles between framework grains. Intergranular porosity preservation in a sandstone is a function how much intergranular volume has been destroyed by compaction and/or occluding cement by diagenetic events during the burial process. An IGV plot can be useful in the study of diagenetic porosity modification. The plot is used to separate the effects of compaction from the effects of cementation in an attempt to illustrate which of the two diagenetic processes is the dominant causes of porosity loss (Houseknecht, 1987). IGV calculated from the point count data collected in this study is shown in Table 4 and illustrated in Fig. 19.

In the Bay du Nord L-76z well the IGV data shows the Ti-3 incised valley sandstones to have IGV values ranging from 29 to 33%. The Ti-2 incised valley sandstones have IGV values that range from 22 to 41%. These well preserved intergranular volumes suggest that mechanical and chemical compaction played a very small role in porosity reduction of these sandstones. Only minor porosity loss can be attributed to compaction (Fig. 19). The main mechanism for porosity loss is early precipitation of calcite cement that halts the affects of mechanical compaction. However, the high IGV in both sandstone units is a function

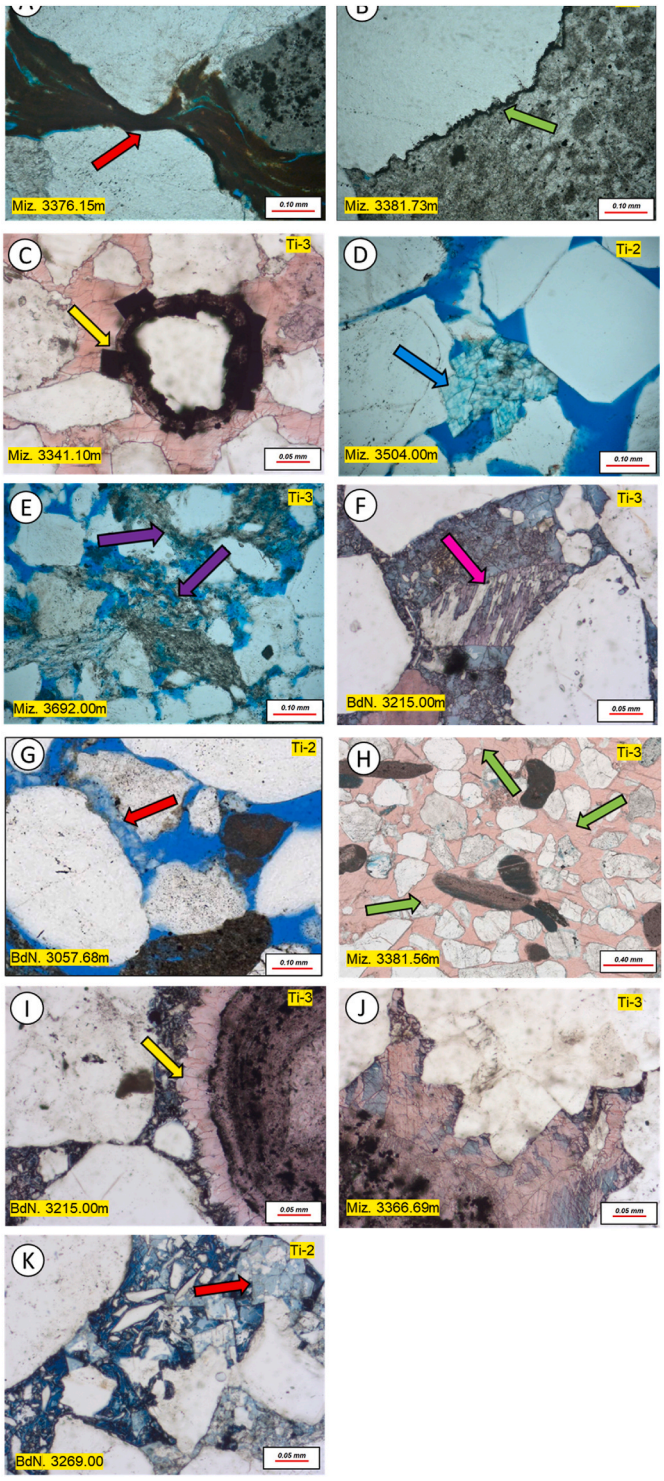

Fig. 17. Diagenetic events in the Ti-2 and Ti-3 incised valley sandstones from Bay du Nord L-76z and Mizzen F-09.3 Digenesis Stage (%Ro= <0.5; from the sediment/water interface up to 50–60 °C). A) Rare ductile rock fragments have been squeezed into adjacent pore-space by the effects of mechanical compaction (red arrow). B) Rare, sutured grain contacts are caused by chemical compaction of siliceous grains (green arrow). C) Early pyrite is replacing some oolitic grains (yellow arrow). D) Early ferroan dolomite crystals are replacing inherited quartz overgrowth (blue arrow). E) Rare, scattered siderite (purple arrows) is squeezed between quartz grains. F) Feldspar grains have been partially leached then cemented with slightly ferroan calcite (pink arrow). G) Rare kaolinite partially fille some pores (red arrow). H) Poikilotopic non-ferroan calcite cement pervasively fills porosity in this sample (green arrows). I) Fibrous calcite early calcite cement is nucleating from an oolitic grain (yellow arrow). J) Some calcite cement is slightly ferroan (blue) and non-ferroan (pink). K) Dark blue ferroan calcite cement may be a later phase of cement. Note early ferroan dolomite cement (red arrow). (For interpretation of the references to colour in this figure legend, the reader is referred to the Web version of this article.)

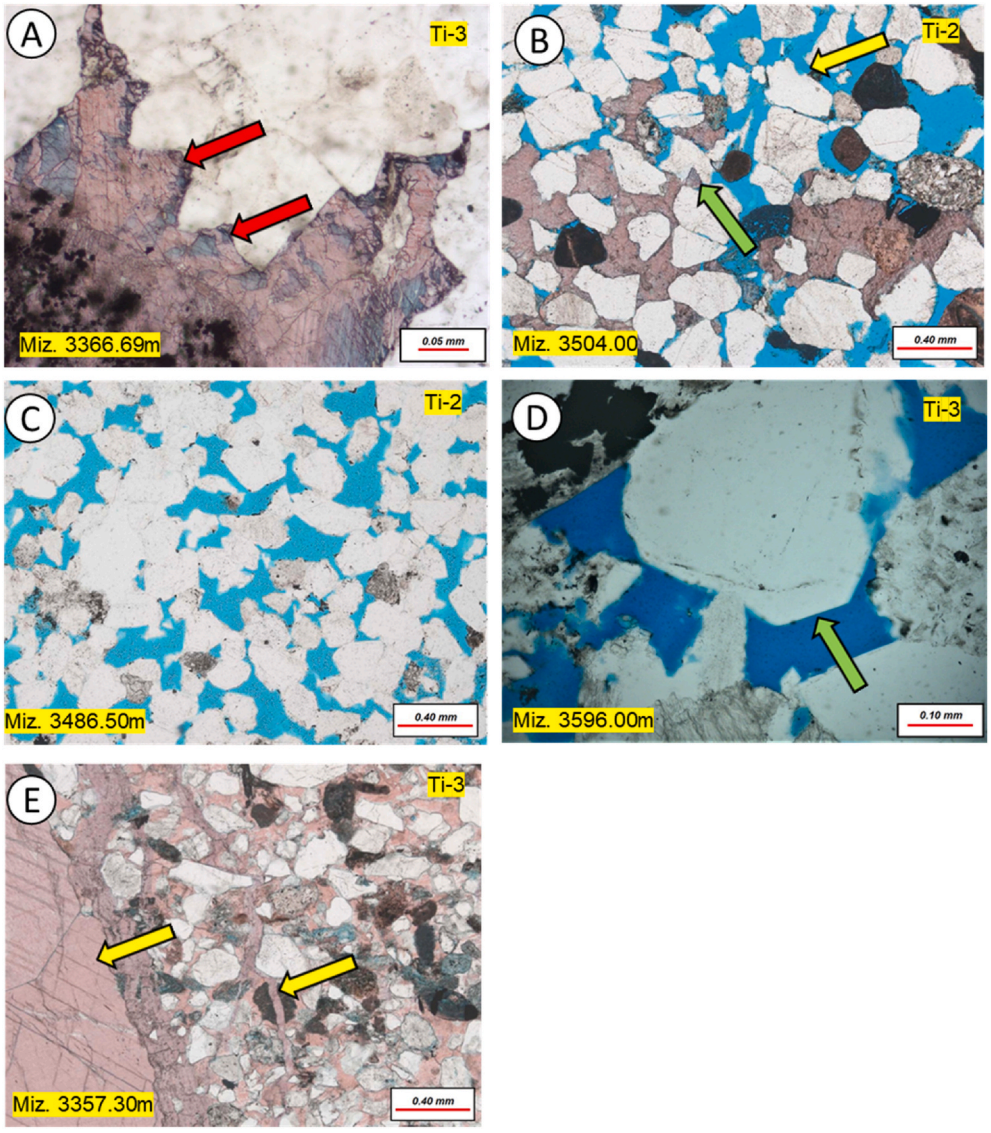

Fig. 18. Diagenetic events in the Ti-2 and Ti-3 incised valley sandstones from Bay du Nord L-76z and Mizzen F-09. Catagenesis Stage (%Ro = 0.5–2.0; intermediate burial from 60 to 140–150 °C). A) Calcite cement is aggressive to silicate grains (red arrow) showing as grain embayment in non-cemented areas. B) Patchy calcite cemented sandstone that calcite cement has been partially dissolved. Green arrow shows grain embayment in cements zone and yellow arrow shows the same texture in a non-cemented zone. C) Excellent example of oversized secondary porosity (blue) after calcite cement dissolution. D) Well developed quartz overgrowth. The euhedral crystal growth suggest it grew *in situ*; however, many quartz overgrowths are inherited from a previous sandstone. E) Rare calcite-healed fractures (yellow arrows) are the latest diagenetic event as the crosscut everything in the sample. (For interpretation of the references to colour in this figure legend, the reader is referred to the Web version of this article.)

of excellent secondary porosity after calcite cement dissolution (23–27% in Ti-3 and 17–27% in Ti-2).

In Mizzen F-09 the Ti-3 incised valley sandstones IGV values range from 29 to 38%. The Ti-2 sandstones IGV values range from 27 to 35%. The IGV is well preserved in these sandstones similar to Bay du Nord L-76z. However, much of the intergranular volume and original porosity loss in the Ti-3 incised valley sandstone is attributed to early precipitation of calcite cement that is still persevered and has not fully dissolved (7–31%; Avg. 26%) that severely reduces reservoir quality in this unit. The intergranular volume in the Ti-2 incised valley sandstone is almost all secondary porosity after calcite dissolution (4–24%; Avg. 17%), with localized calcite cement ranging from 5 to 31% (Avg. 12%). The effects of mechanical and chemical compaction played a very small role in porosity reduction of these sandstones (Fig. 19). However, the dissolution event that occurred at Bay du Nord L-76z was not as prominent at Mizzen F-09 as evident by the preservation of pore occluding calcite cement.

5. Discussion

5.1. Secondary porosity development

Two possible models for the dissolution of early calcite cements are suggested in this study that created the secondary porosity in the Ti-2 and Ti-3 incised valley sandstones: i) SCCA that were expelled during the maturation of organic matter in the late diagenetic to early catagenetic stage leached the early carbonate cements, ii) dissolution caused by meteoric waters entering the incised valley sandstone bodies through unconformities.

5.2. Thermal maturity and dominance of SCCA

The thermal succession for generation of the SCCA from OM begins at approximately 50–60 °C and these acids are a major source of H+ in formation water that can contribute to calcite cement dissolution (Carothers and Kharaka, 1978; Surdam et al., 1984; Crossley et al., 1986; Lundegard and Land, 1986). Carothers and Kharaka (1978) showed that there is a notable increase in organic acid concentrations in formation water at temperatures above 80 °C. Huan et al. (2021) have shown in their experimental data from offshore Bohai Bay Basin, China that SCCA generation in mudstones starts at a temperature of approximately 60 °C. Sanei et al. (2020; unpublished) have shown by adding acetic acid to chalk samples from the Danish North Sea under reservoir conditions (2650 psi and 90 °C) that carbonate dissolution was possible. The study concluded that a dissolution rate of 5.0E-08 to 8.0E-08 g mol/s.cm occurred in the chalk samples within first 10 min of acid-rock

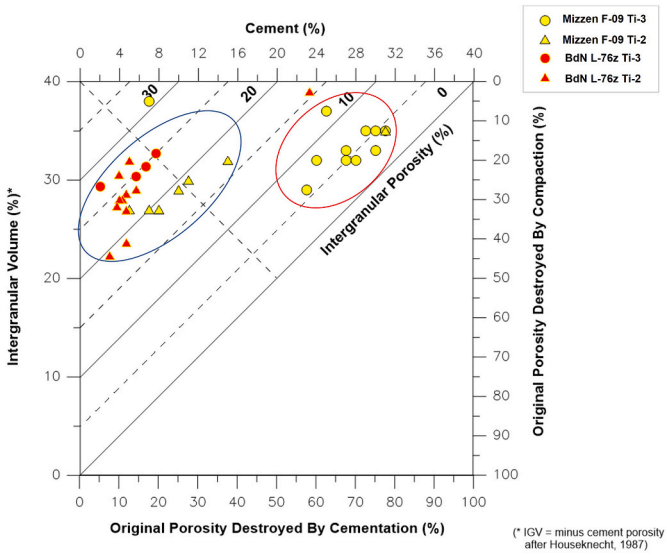

Fig. 19. Intergranular volume (IGV) plot shows the Ti-3 incised valley sandstones in Mizzen F-09 to have high preserved IGV by the high volume of calcite cementation. Red circle indicates samples where porosity has been destroyed mainly by calcite cement. Blue circle indicates samples with high preserved IGV, but in this case the high IGV is secondary porosity after calcite cement dissolution. Compaction has played a very small role in the porosity destruction of these samples. (For interpretation of the references to colour in this figure legend, the reader is referred to the Web version of this article.)

interaction. MacGowan and Surdam (1987) indicate that the specific temperature of SCCA generation is likely basin specific and not a global acid generation temperature because several studied formation waters contain significant SCCA concentrations below 80 °C. Central to these observations is the main phase of SCCA generation is prior to liquid hydrocarbon generation, regardless of fixed empirical temperature ranges (Surdam et al., 1984). In the early diagenetic stage anaerobic bacteria are capable of consuming the SCCA effectively. However, as the bacterial activity is reduced at higher temperatures (50–60 °C) in the late diagenetic and early catagenesis zones, the SCCA becomes dominant in formation water and can accumulate in volume over geologic time (Sanei et al., 2020; unpublished).

The thermal maturity data (%VRo = 0.50) from this study are consistent with the pre-oil generation window and the onset of SCCA from thermal maturation of the Type II OM within the deltaic siltstones/mudstones and the Type II OM within the incised valley sandstones. It is evident from the organic petrology, thermal maturity data, and petrographic observations from this study that SCCA's have played a significant role in secondary porosity generation by dissolution of early calcite cement. Porous zones in the Ti incised valley sandstones are in close proximity to abundant thin interbedded muddy organic-rich laminae (Fig. 20). The incised valleys interpreted from core and wireline logs are not necessarily situated in the valley axis (refer to Fig. 3). They appear to only cut down to a point above the MFS and this may not be the case laterally where they may have eroded deeper. Therefore, the Type II lamalginite OM were likely deposited when the incised valley was cut into the MFS of the underlying (older) sequence. Large clasts of HI-rich lamalginite strata where then redistributed within the fluvial incised valley deposits. Further, lamalginites associated within the thin muddy

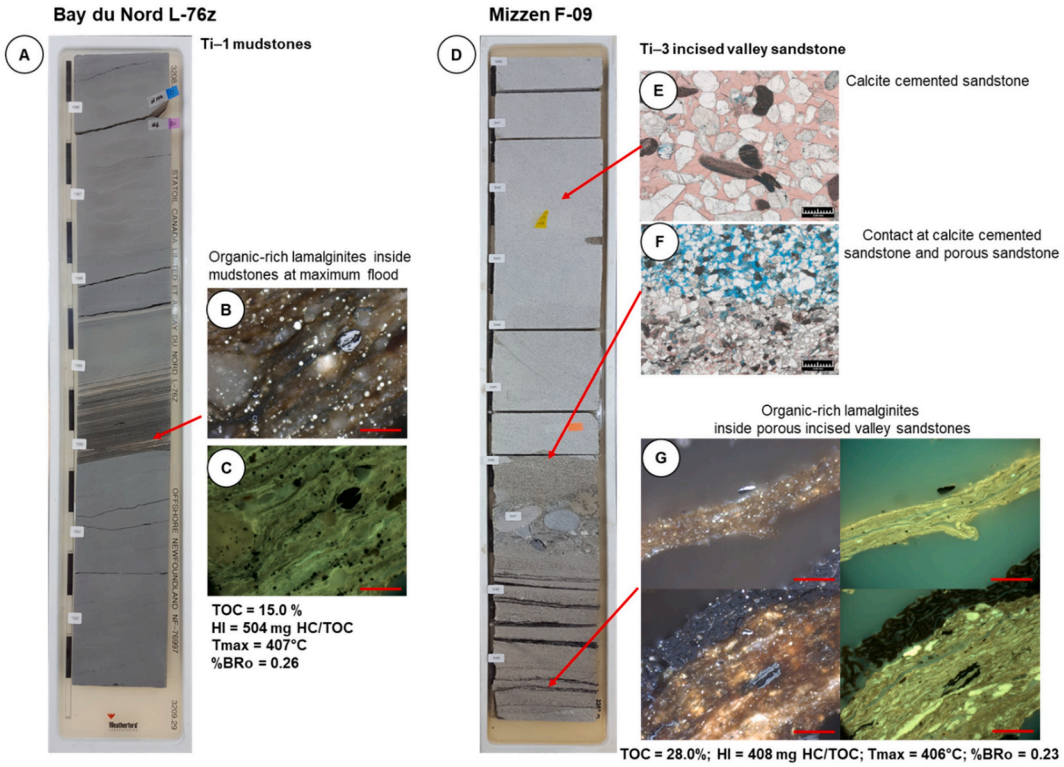

Fig. 20. A) Core photograph showing a cm-thick bed of organic-rich lamalginites at a MFS. B) Organic petrology photomicrograph showing a close view of a mixture of dark brown layers of lamalginite. C) Same field of view as in B, but in fluorescence showing bright green fluorescing lamalginite. D) Core photographs of the Ti-3 incised valley sandstone in Mizzen F-09 showing the contact between a calcite cemented zone and porous sandstone. E) Pervasive calcite cement (pink stained area in thin section photomicrograph) in zones where organic matter is absent (grey area on core). F) Close view of contact between calcite cement and secondary porosity (blue area in thin section photomicrograph) in association with organic matter suggesting thermal maturation of SCCA caused dissolution of calcite cement during the late diagenesis to early catagenesis stage at approximately 60 °C (%VRo = 0.50). G) Organic petrology photomicrographs showing a mixture of dark brown layers of lamalginite and well preserved bituminite. Minor highly reflecting Zooclasts are also present. Photos on the right are the same field of view, but in fluorescence. (For interpretation of the references to colour in this figure legend, the reader is referred to the Web version of this article.)

lamina may be indicative of a tidal-influenced depositional environment (Fig. 20). It likely the OM was gently reworked and redeposited along with the muddy laminae. Reworking of the OM may explain the slightly lower HI values associated in the OM deposited within the incised valley sandstones compared to similar lamalginites associated with the MFS within the deltaic mudstones. Stewart (2016; unpublished) noted a lack of bioturbation in the incised valley sandstones indicating a lack of biological activity promoting further preservation of the Type II OM until progressive transgression filled the valley with deltaic sediments. It is suggested here that SCCA were generated from OM, during maturation, in the mudstones enveloping the Ti-2 and Ti-3 incised valley sandstones and OM present within the incised valley sandstones. Therefore, it is evident that the onset and eventual accumulation of SCCA at %VRo = 0.50; 60 °C created significant secondary porosity by the dissolving early calcite cement.

5.3. Meteoric water flushing

Secondary porosity from carbonate dissolution related to meteoric water flushing has been reported in other basins by several workers (Khidir and Catuneanu, 2003; Poursoltani and Gibling, 2011; Zaid, 2021; Yuan et al., 2017). Many world-class paleokarst carbonate reservoirs developed below unconformities where carbonates underwent subaerial exposure to meteoric waters for long periods of time that created significant secondary porosity volumes (e.g., Dembicki and Machel, 1996, Dou et al., 2017). Dissolution caused by meteoric water flushing in sandstones has been reported in reservoirs at burial depths greater than 3 km (Bjørlykke et al., 2017). Permeable aquifers and open fracture networks can act as conduits for meteoric water to enter into marine basins and meteoric water dissolution of minerals such as calcite and feldspar are highest near the tops of reservoir sands close to the area of recharge (Bjørlykke and Jahren, 2012). How much carbonate cement that can removed is a function paleoclimate, groundwater table slope, hydraulic head, and lateral continuity of the aquifers delivering the meteoric water to the buried sand body (Bjørlykke et al., 2017).

Several rifting events during Jurassic sedimentation in the offshore Newfoundland area have been previously reported (Foster and Robson, 1993; Sinclair et al., 1994; Magoon et al., 2005). Numerous subaerial unconformities during sea level low stand and subsequent transgression deposition of the Ti incised valley sandstones in the Flemish Pass have been described in core and inferred from wireline logs (Stewart, 2016; unpublished). During uplift and exposure, the buried Ti incised valley sandstones may be in close proximity to these unconformities (refer to Fig. 3). However, due to high structural accommodation in the Flemish Pass the incised valley sandstones likely stay buried even during subsequent structural uplift (Stewart, 2016; unpublished). This would imply that the Ti incised valley sandstones were breached by a younger deeply cut incised valley that cut through all of the overlying strata. Alternatively, the base Cretaceous unconformity may cut through all of the Ti sequences allowing meteoric water to enter the incised valley sandstones though the secondary pore network created by the SCCA further removing early calcite cement. However, there is very little evidence from core or wireline logs that either of these meteoric water flushing events have occurred. 3-D seismic sections of the area would need to be examined to verify if the stacked Ti incised valley sandstones were exposed along unconformity boundaries to allow meteoric water to enter the sandstone bodies.

6. Conclusion

In this study we used thin section petrography, programmed pyrolysis, and organic petrology to understand the diagenetic controls of the anomalously high secondary porosity in deeply buried (2-3 Km), Tithonian-aged (Ti) sandstone reservoirs in two wells from the Flemish Pass area offshore Newfoundland. Detailed petrographic analysis showed that the anomalously high secondary porosity is the result of dissolution of an early pervasive calcite cement phase. Programmed pyrolysis data combined with organic petrology results showed all the organic macerals found in the deltaic siltstone, mudstones, and interlaminated mudstones within the stacked incised valley sandstones to be immature Type II alginite and Type III organic mater. Thermal maturity data measured on a subset of organic macerals confirmed the Type II organic matter to be in the late diagenesis to early catagenesis stage (% VRo = 0.50; 60 °C). This thermal maturity is consistent with the pre-oil generation window and the onset of SCCA. Therefore, it is evident that SCCA's have played a significant role in secondary porosity generation by dissolution of early calcite cement in the wells from this study. Meteoric water flushing was examined as a second mechanism of early carbonate cement dissolution. However, insignificant data control was available to verify this as a viable mechanism for calcite cement dissolution. 3-D seismic would aid in identifying regional-scale unconformities that could cut through the Ti sequences to supply meteoric waters to the incised valley sandstone units.

Declaration of competing interest

The authors declare that they have no known competing financial interests or personal relationships that could have appeared to influence the work reported in this paper.

Acknowledgements

We are extremely grateful to Dr. Omid H. Ardakani from the Geological Survey of Canada for the use of their lab facilities as well as Dr. W.D. Stewart (Husky Energy Inc.; retired) for providing insights on sequence stratigraphy. The manuscript improved greatly with suggestions supplied from Dr Wahid Rahman (GPR Inc.) and an anonymous reviewer.

Appendix A. Supplementary data

Supplementary data to this article can be found online at https://doi.org/10.1016/j.marpetgeo.2022.105644.

References

Beicip-Franlab, 2015. Offshore Newfoundland & Labrador Resource Assessment Flemish Pass Area NL15_01EN. An Integrated Project for. Nalcor Energy – Oil and Gas Inc. Department of Natural Resources, Government of Newfoundland and Labrador.

Beicip-Franlab, 2018. Offshore Newfoundland & Labrador Resource Assessment Orphan Basin Area NL18-CFB01. An Integrated Project for. Nalcor Energy – Oil and Gas Inc. Department of Natural Resources, Government of Newfoundland and Labrador.

Bjørlykke, K., Line, L.H., Jahren, J., Mondol, N.H., Aagaard, P., Hellevang, H., 2017. Compaction of Sand and Clay - Constraints from Experimental Compaction, Chemical Reactions and Fluid Flow during Burial - an Overview. Search and Discovery article 51449.

Bjørlykke, K., Jahren, J., 2012. Open or closed geochemical systems during diagenesis in sedimentary basins: constraints on mass transfer during diagenesis and the prediction of porosity in sandstone and carbonate reservoirs. AAPG (Am. Assoc. Pet. Geol.) Bull. 96 (12), 2193–2214, 2012.

Blamey, N.J.F., Azmy, K., Brand, U., 2014. Provenance and burial history of cement in sandstones of the Northbrook Formation (Carboniferous), western Newfoundland, Canada: a geochemical investigation. Sediment. Geol. 30–41.

Burley, S.D., Worden, R.H., 2003. Sandstone Diagenesis: Recent and Ancient. Blackwell Publishing Ltd., Oxford, United Kingdom, p. 649.

Burley, S.D., Kantorowicz, J.D., 1986. Thin section and S.E.M. textural criteria for the recognition of cement-dissolution porosity in sandstones. Sedimentology 33, 587–604.

Caplan, M.L., Moslow, T.F., 1998. Paragenetic evolution of reservoir facies, middle triassic halfway formation, peejay field, northeastern British columbia: controls on reservoir quality. Bull. Can. Petrol. Geol. 46 (3), 424–444.

Carothers, W.W., Kharaka, Y.K., 1978. Aliphatic acid anions in oil field waters—implications for origin of natural gas. AAPG (Am. Assoc. Pet. Geol.) Bull. 62, 2441–2453.

Creaney, S., Allison, B.H., 1987. An organic geochemical model of oil generation in the Avalon/Flemish Pass sub-basins, east coast Canada. Bull. Can. Petrol. Geol. 35 (1), 12–23.

Dembicki, E.A., Machel, H.G., 1996. Recognition and delineation of paleokarst zones by the use of wireline logs in the bitumen-saturated Upper Devonian Grosmont

Formation of Northeastern Alberta, Canada. AAPG (Am. Assoc. Pet. Geol.) Bull. 80 (5), 695–712.
DeSilva, N.R., 1999. Sedimentary basins and petroleum systems offshore Newfoundland and Labrador. In: Fleet, A.J., Boldy, S.A.R. (Eds.), Petroleum Geology of Northwest Europe: Proceedings of the Fifth Conference. The Geological Society, London, pp. 501–515.
Dickinson, W.R., 1985. Interpreting provenance relations from detrital modes of sandstones. In: Zuffa, G.G. (Ed.), Provenance of Arenites. Reidel, Dordrecht, pp. 333–361.
Dou, W., Liu, L., Wu, K., Xu, Z., Feng, X., 2017. Origin and significance of secondary porosity: a case study of upper Triassic tight sandstones of Yanchang Formation in Ordos basin, China. J. Petrol. Sci. Eng. 149, 485–496.
Enachescu, M.E., 1987. Tectonic and structural framework of Northeast Newfoundland central margin, Sedimentary basins and basin forming mechanisms. In: Beaumont, C., Tankard, A.J. (Eds.), Canadian Society of Petroleum Geologists, Memoir 12, vol. 5. Atlantic Geoscience Society Special Publications, pp. 117–146.
Enachescu, M.E., 2005. In: Offshore Newfoundland and Labrador: an Emerging Energy Powerhouse. Offshore Technology Conference Paper #17570, p. 8p. Houston, Texas.
Enachescu, M.E., Hogg, J.R., Fowler, M., Brown, D.E., Atkinson, I., 2010. Late jurassic source rock super-highway on conjugate margins of the North and central atlantic (offshore east coast Canada, Ireland, Portugal, Spain and Morocco). CM 2010-Abstracts 2.
Enachescu, M., 2012. Petroleum Exploration Opportunities in the Flemish Pass Basin. Call for Bids NL12-02, Parcel 1. http://www.nr.gov.nl.ca/nr/invest/call_bids_petro_exploration_enachescu%20.pdf.
Folk, R.L., 1980. Petrology of Sedimentary Rocks. Hemphill Publishing Company, Austin, Texas, p. 184p.
Foster, D.G., Robson, A.G., 1993. Geological history of the flemish Pass Basin, offshore Newfoundland. AAPG (Am. Assoc. Pet. Geol.) Bull. 77 (4), 588–609.
Fowler, M.G., McAlpine, K.D., 1995. The Egret member, a prolific kimmeridgian source rock from offshore eastern Canada. In: Katz, B.J. (Ed.), Petroleum Source Rocks. Casebooks in Earth Sciences. Springer, Berlin, Heidelber.
Fowler, M.G., Snowdon, L.R., Stewart, K.R., McAlpine, K.D., 1990. Rock-Eval/TOC data from nine wells located offshore Newfoundland. Geol. Surv. Can. Open File Rep. 2271, 72.
Fowler, M.G., Snowdon, L.R., Stewart, K.R., McAlpine, K.D., 1991. Rock-Eval/TOC data from five wells located within Jeanne d'Arc Basin. offshore Newfoundland GeoL Surv. Can. Open File Rep. 2392, 41.
Fowler, M.G., Obermajer, M., Achal, S., Milovic, M., 2007. Results of Geochemical Analyses of an Oil Sample from Mizzen L-11 Well, Flemish Pass, Offshore Eastern Canada. Open-File Report - Geological Survey of Canada.
Frank, J.R., Carpenter, A.B., Oglesby, T./W., 1982. Cathodoluminescence and composition of calcite cement in the taum sauk limestone (upper cambrian), southeast Missouri. J. Sediment. Res. 52 (2), 631–638.
Gluyas, J., Coleman, M., 1992. Material flux and porosity changes during sediment diagenesis. Nature 356 (6364), 52–54.
Gordon, J.B., Sanei, H., Ardakani, O.H., Pedersen, P.K., 2021. Effect of Sediment Source on Source Rock Hydrocarbon Potential; an Example from the Kimmeridgian and Tithonian-Aged Source Rocks of the Central Ridge, Off-Shore Newfoundland, Canada, vol. 127. Marine and Petroleum Geology.
Haile, B.G., Line, L.H., Klausen, T.G., Olaussen, S., Eide, C.H., Jahren, J., Hellevang, H., 2020. Quartz overgrowth textures and fluid inclusion thermometry evidence for basin-scale sedimentary recycling: an example from the Mesozoic Barents Sea Basin. Basin Res. 33 (3).
Hansley, P.L., Nuccio, V.F., 1992. Upper cretaceous shannon sandstone reservoirs, powder river basin, Wyoming: evidence for organic acid diagenesis. AAPG (Am. Assoc. Pet. Geol.) Bull. 76 (6), 781–791.
Haynes, S.R., Marshall, J., Wathne, E.I., Minielly, G., Mortlock, E., Walderhaug, O., Johnson, T., 2014. Depositional Interpretation and Reservoir Characterization of the Tithonian in Mizzen F-09, Flemish Pass Basin. Canada. Search and Discovery. Article #50967.
Hesse, R., Abid, I.A., 1998. Carbonate cementation: key to reservoir properties of four sandstone levels (cretaceous) in the Hibernia oilfield, Jeanne D'Arc Basin, Newfoundland, Canada. In: Morad, S. (Ed.), Carbonate Cementation in Sandstones. Blackwell Publishing Ltd, pp. 363–393.
Horsfield, B., Rullkötter, J., 1994. Diagenesis, Catagenesis, and Metagenesis of Organic Matter. The Petroleum System—From Source to Trap. Leslie B. Magoon, Wallace G. Dow.
Houseknecht, D.W., 1987. Assessing the relative importance of compaction processes and cementation to reduction of porosity in sandstones. AAPG (Am. Assoc. Pet. Geol.) Bull. 71 (6), 633–642.
Huan, L., Qingbin, W., Xiaofeng, D., Xianghua, Y., Hongtao, Z., 2021. Residual carboxylic acids (nonpyrolytic) in mudstones and their implications and constraints on sandstone diagenesis, Bozhong Depression, offshore Bohai Bay Basin, East China. Org. Geochem. 151, 104–149.
Huang, Z., 1994. Predicted and measured petrophysical and geochemical characteristics of the Egret Member oil source rock, Jeanne d' Arc Basin, Offshore Eastern Canada. Mar. Petrol. Geol. 11, 294–306.
ICCP, 1998. The new vitrinite classification (ICCP System 1994). Fuel 77, 349–358.
ICCP, 2001. The new inertinite classification (ICCP System 1994). Fuel 80, 459–471.
Jarvie, D.M., 2012. Shale resource systems for oil and gas: Part 1 – shale oil resource systems. In: Breyer, J. (Ed.), Shale Reservoirs – Giant Resources for the 21st Century, vol. 97. AAPG Memoir, pp. 1–19.
Khidir, A., Catuneanu, O., 2003. Sedimentology and diagenesis of the scollard sandstones in the red deer valley area, central Alberta. Bull. Can. Petrol. Geol. 51 (1), 45–69.
Lafargue, E., Marquis, F., Pillot, D., 1998. Rock-Eval 6 applications in hydrocarbon exploration, production and soil contamination studies. Rev. Inst. Fr. Petrol 53 (4), 421–437.
Loucks, R.G., Patty, K., 2017. Vadose Diagenetic Dissolution Textures, Cementation Patterns, and Aragonite and Mg–Calcite Alteration in the Holocene Isla Cancún Eolianite Aragonitic Ooids: Modern Analog for Ancient Ooid-Grainstone Pore Networks. GCAGS Explore & Discover. Article #00272.
Lundegard, P.D., Land, L.S., Galloway, W.E., 1984. Problem of secondary porosity: frio formation (oligocene), Texas gulf coast. Geology 12 (7), 399–402.
MacGowan, D.B., Surdam, R.C., 1987. Dysfunctional carboxylic acid anions in oilfield waters. Org. Geochem. 12 (3), 245–259.
Machel, H.G., 1985. Cathodoluminescence in calcite and dolomite and it's chemical interpretation. Geosci. Can. 12, 139–147.
Magoon, L.B., Hudson, T.L., Peters, K.E., 2005. Egret-Hibernia(!), a significant petroleum system, northern Grand Banks area, offshore eastern Canada. AAPB Bulletin 89 (9), 1203–1237.
May, R.W., 1980. The formation and significance of irregularly shaped quartz grains in till. Sedimentology 27, 325–331.
Olanipekun, B., Azmy, K., 2021. Carbonate cementation in the tithonian Jeanne d'Arc sandstone, terra nova field, Newfoundland: implications for reservoir quality evolution. Sedimentology.
Paxton, S.T., Szabo, J.O., Ajdukiewicz, J.M., Klimentidis, R.E., 2002. Construction of an intergranular volume compaction curve for evaluating and predicting compaction and porosity loss in rigid-grain sandstone reservoirs. AAPG (Am. Assoc. Pet. Geol.) Bull. 86 (12), 2047–2067.
Pickel, W., Kus, J., Flores, D., Kalaitzidis, S., Christanis, K., Cardott, B.J., Misz-Kennan, M., Rodrigues, S., Hentschel, A., Hamor-Vido, M., Crosdale, P., Wagner, N., 2017. Classification of liptinite – ICCP system 1994. Int. J. Coal Geol. 169.
Poursoltani, M.R., Gibling, M.R., 2011. Composition, porosity, and reservoir potential of the middle jurassic kashafrud formation, northeast Iran. Mar. Petrol. Geol. 28, 1094–1110.
Raine, R., 2006. Petrographical analyses and depositional environmental interpretation of laminated mudrocks from well L-76Z, Bay du Nord, offshore Newfoundland. Internal report prepared for Statoil Canada Limited.
Sanei, H., Yoo, H., Rudra, A., Lee, J., 2020. Can We Use the Naturally Produced Acetates in the Lower Cretaceous Shale as Scale Inhibitor? (Unpublished.
Sanei, H., 2020. Genesis of solid bitumen. Sci. Rep. 10, 15595.
Schmidt, V., Mcdonald, D.A., 1979. The Role of Secondary Porosity in the Course of Sandstone Diagenesis, vol. 26. SEPM Special Publication, pp. 175–207.
Sinclair, I.K., Shannon, P.M., Williams, B.P.J., Harker, S.D., Mooren, J.G., 1994. Tectonic control on sedimentary evolution of three North Atlantic borderland Mesozoic basins. Basin Res. 6 (4).
Sommer, S.E., 1972. Characterization of cathodoluminescence from carbonate solid solutions. Chem. Geol. 9, 257–273.
Stewart, W.D., 2016. Sedimentological interpretations, sequence stratigraphic context, and exploration potential of Latest Tithonian depositional systems, Bay du Nord and Mizzen areas, Flemish Pass Basin, offshore Newfoundland. Husky Energy internal report (Unpublished.
Stück, H., Koch, R., Siegesmund, S., 2013. Petrographical and petrophysical properties of sandstones: statistical analysis as an approach to predict material behaviour and construction suitability. Environ. Earth Sci. 69, 1299–1332.
Surdam, R.C., Crossey, L.J., 1985. Organic-inorganic reactions during progressive burial: key to porosity and permeability enhancement and preservation. Philos. Trans. R. Soc. London, Ser. A 315, 135–156.
Surdam, R.C., Boese, S.W., Crossey, L.J., 1984. The chemistry of secondary porosity. AAPG Memoir 37 (2), 183–200.
Swift, J.H., Williams, J.A., 1980. Petroleum source rocks, grand banks area. In: Miall, A. D. (Ed.), Facts and Principles of World Petroleum Occurrence: Canadian Society of Petroleum Geologists Memoir 6, pp. 567–587.
Taylor, T.R., Giles, M.M., Hathon, L.V., Diggs, T.N., Braunsdorf, N.R., Birbiglia, G.V., Kitteridge, M.G., Macaulay, C.I., Espejo, I.S., 2010. Sandstones and reservoir-quality prediction: models, myths, and reality. AAPG (Am. Assoc. Pet. Geol.) Bull. 94, 1093–1132.
Teal, C.S., Mazzullo, S.J., Bischoff, W.D., 2000. Dolomitization of Holocene shallow-marine deposits mediated by sulfate reduction and methanogenesis in normal-salinity seawater, Northern Belize. J. Sediment. Res. 70 (3), 649–663.
Vandeginste, V., John, C.M., 2012. Influence of climate and dolomite composition on dedolomitization: insights from a multi-proxy study in the central Oman Mountains. J. Sediment. Res. 82 (3), 177–195.
Xiong, D., Azmy, K., Blamey, N., 2016. Diagenesis and origin of calcite cement in the Flemish Pass Basin sandstone reservoir (Upper Jurassic): implications for porosity development. Mar. Petrol. Geol. 70 (10), 1016.
Yuan, G., Cao, Y., Zhang, Y., Gluyas, J., 2017. Diagenesis and reservoir quality of sandstones with ancient "deep" incursion of meteoric freshwater - an example in the Nanpu Sag, Bohai Bay Basin, East China. Mar. Petrol. Geol. 82, 444–464.
Yuan, G.H., Cao, Y.C., Gluyas, J., 2019. How important is carbonate dissolution in buried sandstones: evidences from petrography, porosity, experiments, and geochemical calculations? Petrol. Sci. 16, 729–751.
Yuan, G., Cao, Y., Schulz, H.M., Hao, F., Gluyas, J., Liu, k., Yang, T., Wang, Y., Xi, K., Li, F., 2019. A review of feldspar alteration and its geological significance in sedimentary basins: from shallow aquifers to deep hydrocarbon reservoirs. Earth Sci. Rev. 191, 114–140.
Zaid, S.M., 2021. Provenance, diagenesis, tectonic setting and geochemistry of rudies sandstone (lower miocene), warda field, gulf of suez, Egypt. J. Afr. Earth Sci. 66, 65–71. –67.